# Simulating oxygen isotope ratios in tree ring cellulose using a dynamic global vegetation model

**S. G. Keel[1*], F. Joos[1], R. Spahni[1], M. Saurer[2], R. B. Weigt[2], S. Klesse[3,4]**

[1]{University of Bern, Physics Institute, Climate and Environmental Physics & Oeschger Centre for Climate Change Research, Bern, Switzerland}

[2]{Paul Scherrer Institute, Laboratory of Atmospheric Chemistry, Villigen, Switzerland}

[3] {Swiss Federal Research Institute WSL, Birmensdorf, Switzerland}

[4] {Oeschger Centre for Climate Change Research, Bern, Switzerland}

[*]{now at: Agroscope, Institute for Sustainability Sciences, Climate and Air Pollution, Zurich, Switzerland}

Correspondence to: S. G. Keel (sonja.keel@agroscope.admin.com)

## Abstract

Records of stable oxygen isotope ratios in tree rings are valuable tools to reconstruct past climatic conditions and the response of trees to those conditions. So far the use of stable oxygen isotope signatures of tree rings has not been systematically evaluated in dynamic global vegetation models (DGVMs). DGVMs integrate many hydrological and physiological processes and their application could improve proxy-model comparisons and the interpretation of oxygen isotope records. Here we present an approach to simulate leaf water and stem cellulose $\delta^{18}O$ of trees using the LPX-Bern DGVM (LPX-Bern). Our results lie within a few per mil of measured tree ring $\delta^{18}O$ of thirty-one different forest stands mainly located in Europe. Temporal means over the last five decades as well as inter-annual variations for a subset of sites in Switzerland are captured. A sensitivity analysis reveals that relative humidity, temperature, and the water isotope boundary conditions have the largest influence on simulated stem cellulose $\delta^{18}O$, followed by all climatic factors combined, whereas increasing atmospheric $CO_2$ and nitrogen deposition exert no

impact. We conclude that simulations with LPX-Bern are useful to investigate large-scale oxygen isotope patterns of tree-ring cellulose, to elucidate the importance of different environmental factors on isotope variations and therefore help to reduce uncertainties in the interpretation of $\delta^{18}O$ of tree-rings.

## 1 Introduction

Stable oxygen isotope ratios ($^{18}O/^{16}O$) are widely used to reconstruct past climatic conditions and to characterize the modern hydrological cycle. $\delta^{18}O$ ($\delta^{18}O = [((^{18}O/^{16}O)_{sample}/(^{18}O/^{16}O)_{standard})-1] * 1000$ [‰]) is routinely measured in various climate archives such as ice cores (Dansgaard, 1964; Johnsen et al., 2001; Jouzel et al., 2003; Severinghaus et al., 2009), speleothems (Fleitmann et al., 2004; McDermott, 2004), corals (Dunbar et al., 1994), ocean sediments (Shackleton and Obdyke, 1973; Elderfield and Ganssen, 2000), and tree rings (Libby et al., 1976; Treydte et al., 2006) as well as in modern precipitation samples (Rozanski et al., 1992; Kern et al., 2014). Regarding the tree ring archive, recent efforts were directed to document $\delta^{18}O$ variability in stem cellulose from tree ring samples over the last millennium (e.g. Masson-Delmotte et al., 2005; Treydte et al., 2006; Edwards et al., 2008) and the industrial period (Anderson et al., 1998; Miller et al., 2006). The spatial distribution of tree ring $\delta^{18}O$ has been characterized across large areas (e.g. Saurer et al., 2002; Herweijer et al., 2007; Treydte et al., 2007). In addition, attempts have been made to unravel the processes that determine stem cellulose $\delta^{18}O$ (e.g. Gessler et al., 2009; Offermann et al., 2011).

The cycling of water isotopes through the climate system including the transfer of water associated with gross primary productivity on land was successfully implemented in atmospheric general circulation and in Earth System Models (Joussaume et al., 1984; Jouzel et al., 1987; Hoffmann et al., 1998; Noone and Simmonds, 2002; Sturm et al., 2005; Werner et al., 2011) to characterize the hydrological cycle. Model results are used to demonstrate that the El Niño Southern Oscillation imprints a pronounced signal on water isotopes (Hoffmann et al. 1998), to reconstruct past precipitation patterns (Risi et al., 2010; Sjolte et al., 2011; Masson-Delmotte et al., 2015), and to explain $\delta^{18}O$ paleo data (Hoffmann et al., 2003). Model results are evaluated against stable isotope ratios in precipitation (Joussaume et al., 1984), snow (Jouzel et al., 1987),

ground water (Hoffmann et al., 1998), water vapor (Werner et al., 2011), and ice core $\delta^{18}O$ data (e.g. Risi et al., 2010). Because none of these models describes $\delta^{18}O$ in stem cellulose, a direct model-data comparison is not yet possible for tree rings and global scale models. So far process models describing the transfer of isotopic signals from soil water and water vapor to leaf water, and finally stem cellulose, were applied for single sites only (Roden et al., 2000; Ogée et al. 2009; Kahmen et al., 2011; Treydte et al., 2014). Yet, the implementation of such an approach in large-scale global land biosphere models is missing. A large-scale approach would have the advantage that many hydrological and physiological processes could be integrated and large spatial and temporal patterns could be explored. Furthermore the importance of individual factors such as rising atmospheric $CO_2$ could easily be examined.

The goals of this study are (i) to describe the implementation of the stable water isotope fluxes and pools in the LPX-Bern DGVM, including $\delta^{18}O$ in stem cellulose for direct model-proxy comparison, (ii) to estimate the large-scale spatial distribution of $\delta^{18}O$ in leaf water and stem cellulose, (iii) to quantify the drivers of spatio-temporal trends and variability of stem cellulose $\delta^{18}O$ in the model context and to assist in the interpretation of tree ring $\delta^{18}O$ data, and (iv) to assess the model performance for large-scale spatial gradients, multi-decadal trends, and inter-annual variability with a focus on extra-tropical forests. We compiled time-averaged tree ring $\delta^{18}O$ data from thirty-one boreal and temperate forest sites to capture spatial variability and use five tree-ring-$\delta^{18}O$ records from Switzerland to detail local temporal variability. Soil water and water vapor $\delta^{18}O$ results from transient simulations with the model ECHAM5-JSBACH (Haese et al., 2013) over the past 50 years are used as oxygen isotope input data (i.e. isotope forcing). Factorial experiments at the site scale are performed to identify drivers of decadal trends and inter-annual variability.

## 1.1 Isotope background

Evaporation and condensation are the two processes that predominantly influence water oxygen isotope ratios in the climate system. Water molecules containing the lighter $^{16}O$ isotopes evaporate more readily compared to molecules containing the heavier $^{18}O$. Therefore moisture evaporated from the ocean is depleted in $^{18}O$ compared to ocean water, which has a $\delta^{18}O$ of near zero per mil. As air cools by rising into the atmosphere or moving toward the poles, moisture

85 begins to condense and falls as precipitation. Water vapor molecules containing $^{18}O$ condense
86 more readily and rain is enriched in $^{18}O$ compared to its vapor source. As the air continues to
87 move pole-ward into colder regions (temperature effect) or further inland (continental effect) the
88 remaining moisture in the air as well as the water that condenses and precipitates become
89 increasingly more $^{18}O$ depleted. This is reflected in the spatial distribution of oxygen isotope
90 ratios in soil water and water vapor. The $\delta^{18}O$ of surface soil water reflects the $\delta^{18}O$ signal of
91 precipitation averaged over a certain amount of time and is further modified by evaporation of
92 soil water leading to evaporative enrichment and potentially by mixing with ground water.

93 Plants take up water which carries this precipitation or soil water $\delta^{18}O$ signature. During transport
94 from roots to leaves isotope ratios are not modified (Wershaw et al., 1966). In the leaves, water
95 becomes enriched in $^{18}O$ relative to source water as a result of transpiration (Dongmann et al.,
96 1974). The enrichment at the site of evaporation (the stomata) is primarily driven by the ratio of
97 the vapor pressure outside versus inside the leaf. Source water (i.e. soil water) that enters the leaf
98 via the transpirational stream, mixes with the $^{18}O$-enriched water and dilutes the leaf water $\delta^{18}O$
99 signal (a Péclet effect, Barbour et al., 2004). This Péclet effect tends to reduce the signal of
100 evaporative enrichment in bulk leaf water (i.e. whole leaf water) and the effect is large when
101 transpiration rates are high. Sucrose formed in the leaves is thought to be 27‰ enriched in $^{18}O$
102 compared to leaf water due to fractionation during the exchange of oxygen between carbonyl
103 groups in organic molecule and water (Sternberg et al., 1986). Sugars are then transported down
104 the trunk where partial exchange with xylem water occurs before tree-ring cellulose is formed
105 (Roden et al., 2000; Gessler et al., 2014). Based on isotope theory, oxygen isotope ratios in tree
106 rings serve as proxy data for relative humidity and reflect the signature of soil water (McCarroll
107 and Loader, 2004). The relative strength of the humidity and soil water signal, however, is
108 expected to vary due to the Péclet effect and oxygen isotope exchange during stem cellulose
109 formation (see below) and is often difficult to quantify, which somewhat hampers current
110 interpretation of tree-ring results.

111 Tree ring chronologies have been found to correlate with relative humidity (Burk and Stuiver,
112 1981; An et al., 2014; Xu et al., 2014) and $\delta^{18}O$ of precipitation (Waterhouse et al., 2002). In
113 addition, tree ring $\delta^{18}O$ archives are proxies for e.g. precipitation amounts (Treydte et al., 2006),

the occurrence of droughts (Masson-Delmotte et al., 2005; Herweijer et al., 2007) and tropical cyclones (Miller et al., 2006), or leaf-to-air vapor pressure differences (Kahmen et al., 2011).

Regarding tree rings, $\delta^{18}O$ in stem cellulose has been described with mechanistic models to characterize the transfer of $\delta^{18}O$ signals from soil water to stem cellulose (Roden et al., 2000; Cernusak et al., 2005; Barbour, 2007; Gessler et al., 2009, Ogée et al. 2009). A formulation of leaf water enrichment at the site of evaporation (i.e. the stomata) based on the model by Craig and Gordon (1965) is common to all models, but additional processes related to $\delta^{18}O$ signals in leaf water and stem cellulose are resolved at varying degrees of complexity. Some models include boundary layer considerations (Flanagan et al., 1991) or the Péclet effects that reduce leaf water enrichment (Barbour et al., 2004; Farquhar and Gan, 2003). Others account for variations in isotopic exchange of oxygen with xylem water (Barbour and Farquhar, 2000), or weight diurnal variations in leaf water enrichment by photosynthetic rates (Cernusak et al., 2005). Here, we use a rather general approach with a single Péclet effect and constant isotopic exchange with xylem water, as we aim to simulate stem cellulose across a large range of different species and as we lack detailed species-specific information, e.g. on water flow and the Péclet effect. On the other hand, we move a step forward in that we integrate a mechanistic model for stem cellulose $\delta^{18}O$ into a DGVM that allows us to cover large spatial and temporal scales and that explicitly considers numerous hydrological and physiological processes.

## 2 Material and methods

### 2.1 Model description

Stable oxygen isotopes were implemented in the LPX-Bern DGVM (Land surface Processes and eXchanges, Bern version 1.0) (Spahni et al., 2013; Stocker et al., 2013). LPX-Bern describes the evolution of vegetation cover, carbon (C) and nitrogen (N) dynamics in soil and vegetation, and the exchange of water, $CO_2$, C isotopes, methane, and nitrous oxide between the atmosphere and the land biosphere.

The model version applied here features a horizontal resolution of 3.75 x 2.5 degree, a vertically resolved soil hydrology with heat diffusion and an interactive thawing-freezing scheme (Gerten et

al., 2004; Wania et al., 2009), and features a daily time step for photosynthesis and evapotranspiration. The soil hydrology scheme is similar to a concurrent LPX version (Murray et al., 2011; Prentice et al., 2011). There are ten plant functional types (PFTs) that have distinct bioclimatic limits and differ in their physiological traits such as minimum canopy conductance (Sitch et al., 2003) (Table S2 in Ruosch et al., 2016). The distribution of fine roots in the soil profile is also PFT-specific and leads to competition for water. Light competition is modeled indirectly by assigning a higher mortality to PFTs with a small increment in fractional plant cover and biomass compared to PFTs with a large increment (Sitch et al., 2003). Daily evapotranspiration is calculated for each PFT as the minimum of a plant- and soil-limited supply function ($E_{supply}$) and the demand for transpiration ($E_{demand}$). $E_{supply}$ is the product of root-weighted soil moisture availability and a maximum water supply rate that is equal for all PFTs (Sitch et al., 2003). $E_{demand}$ is calculated following Monteith's (Monteith, 1995) empirical relation between evaporation efficiency and surface conductance,

$$E_{demand} = E_{eq}\, \alpha_m \left[1 - \exp\left(\frac{-g_c\, \phi}{g_m}\right)\right], \quad (1)$$

where $E_{eq}$ is the equilibrium evaporation rate, $g_m$ and $\alpha_m$ are empirical parameters that are equal for all plant functional types, $g_c$ the canopy conductance, and $\phi$ the fraction of present foliage area to ground area (i.e. projected leaf area). Equation (1) is solved for $E_{\text{demand}}$ using the non-water-stressed potential canopy conductance as calculated by the photosynthesis routine for a fixed ratio λ between the $CO_2$ mole fraction in the stomatal cavity and the ambient air. λ is set equal to 0.8 following Sitch et al. (2003) to approximate non-water-stressed conditions and as a starting value for the iterative computation of carbon assimilation and transpiration. In case of water-stressed conditions when $E_{\text{demand}}$ exceeds $E_{\text{supply}}$, canopy conductance and photosynthesis are jointly and consistently down-regulated; $E_{\text{demand}}$ is set to $E_{\text{supply}}$ and Equation 1 is solved for $g_c$.

Photosynthesis is modeled following Collatz et al. (1991; 1992), which is based on the formulations by Farquhar et al. (1980) and Farquhar and von Caemmerer (1982) generalized for global modeling purposes. The N content and Rubisco activity of leaves are assumed to vary seasonally and with canopy position in a way to maximize net assimilation at the leaf level. For $C_3$ plants assimilation is a function of the daily integral of absorbed photosynthetically active

radiation. For a detailed description see Haxeltine and Prentice (1996b, a).

Canopy conductance, $g_c$, is linked to daytime assimilation, $A_{dt}$, through

$$g_c = g_{min} + \frac{1.6A_{dt}}{[c_a(1-\lambda)]}, \quad (2)$$

where $g_{min}$ is a PFT specific minimum canopy conductance and $c_a$ is the ambient mole fraction of $CO_2$ and λ the ratio between the $CO_2$ mole fraction in the stomatal cavity and the ambient air. The equations for water supply and demand, assimilation, and canopy conductance are solved simultaneously by varying λ to yield self-consistent values for λ, $g_c$, assimilation and transpiration.

## 2.2 Leaf water and stem cellulose $\delta^{18}O$ model

To calculate $\delta^{18}O$ in leaf water we use the Péclet modified Craig-Gordon (PMCG) model as described e.g. in Farquhar & Lloyd (1993).

The evaporative enrichment of leaf water above the plant's source water at the site of evaporation ($\Delta^{18}O_e$), is based on the Craig-Gordon formulation (Craig and Gordon, 1965; Dongmann et al., 1974)

$$\Delta^{18}O_e = \varepsilon^+ + \varepsilon_k + (\Delta^{18}O_v - \varepsilon_k)\frac{e_a}{e_i}, \quad (3)$$

where $\varepsilon^+$ is the temperature-dependent equilibrium fractionation factor between liquid and vapor water and is calculated as

$$\varepsilon^+ = 2.644 - 3.206(\frac{10^3}{T_l}) + 1.534(\frac{10^6}{T_l^2})\ (‰), \quad (4)$$

with $T_l$ the leaf temperature in K (Bottinga and Craig, 1969 in Barbour, 2007). $\varepsilon^+$ increases with decreasing temperature and is around 8.8‰ at 30°C and around 11.5‰ at 0°C. $\varepsilon_k$ is the kinetic fractionation factor for water vapor diffusion from the leaf to the atmosphere (32‰; Cappa et al., 2003), $\Delta^{18}O_V$ describes the oxygen isotope enrichment of water vapor in the atmosphere above source water, and $e_a/e_i$ is the ratio of ambient to intercellular vapor pressures. This ratio is equal to relative humidity when leaf and air temperatures are similar and $e_i$ is at saturation pressure. We

assume that leaf temperature is approximated by air temperature (see also Discussion). We use this formulation in LPX-Bern for the comparison against published leaf water $\delta^{18}O$ (West et al., 2008).

All other results were derived with the expanded model that includes a Péclet effect. The Péclet number is defined as

$$\wp = \frac{LE}{cD}, \quad (5)$$

and accounts for the dilution of $^{18}O$-enriched leaf water by unenriched source water that enters the leaf via the transpirational stream ($E$, mol $m^{-2}$ $s^{-1}$) and is effective over a path length $L$ (Farquhar and Lloyd, 1993). To keep the model as simple as possible we set $L$ to 0.03 m for all PFTs following Kahmen et al. (2011), although $L$ can vary largely between species (Kahmen et al., 2009). $c$ is the molar density of water ($55.5 \times 10^3$ mol $m^{-3}$) and $D$ the temperature dependent diffusivity of $H_2{}^{18}O$ in water (Cuntz et al., 2007, Equation A22, Typo corrected: $10^{-8}$ instead of $10^{-9}$):

$$D = 10^{-8} \exp(-0.4 + \frac{1528}{T_l} + \frac{-554368}{T_l^2}) \ (m^2\ s^{-1}) \quad (6).$$

Bulk leaf water $^{18}O$ enrichment can then be calculated as

$$\Delta^{18}O_{LW} = \frac{\Delta^{18}O_e(1 - e^{-\wp})}{\wp} \quad (7)$$

$\Delta^{18}O_{LW}$ is smaller than $\Delta^{18}O_e$ and approaches $\Delta^{18}O_e$ for small transpiration rates $E$. In regions with high leaf transpiration rates such as high latitudes the reduction of $\Delta^{18}O_e$ due to the Péclet effect is most strongly expressed (Fig. S1 in the Supplement). Leaf water $\delta^{18}O$ is

$$\delta^{18}O_{LW} = \Delta^{18}O_{LW} + \delta^{18}O_{SW} \quad (8)$$

where $\delta^{18}O_{SW}$ refers to soil water $\delta^{18}O$. Stem cellulose isotopic composition is calculated as

$$\delta^{18}O_{SC} = p_{ex}p_x(\delta^{18}O_{SW} + \varepsilon_{wc}) + (1 - p_{ex}p_x)(\delta^{18}O_{LW} + \varepsilon_{wc})$$

$$= \delta^{18}O_{SW} + (1 - p_{ex}p_x)\Delta^{18}O_{LW} + \varepsilon_{wc}, \quad (9)$$

where $\varepsilon_{wc}$ is the fractionation between $\delta^{18}O$ of water and the $\delta^{18}O$ of the primary products of

photosynthesis of 27‰ (Epstein et al., 1977), $p_{ex}$ is the proportion of exchangeable oxygen in cellulose formed from sucrose, and $p_x$ is the proportion of $\delta^{18}O_{SW}$ at the site of cellulose formation (Roden et al., 2000). For our simulations we used values of 0.4 for $p_{ex}$ (Cernusak et al., 2005; Sternberg, 2009) and 1.0 for $p_x$ (Kahmen et al., 2011).

Photosynthesis and plant water fluxes and thus changes in leaf water and stem cellulose $\delta^{18}O$ are computed with a daily time step. Because stem cellulose formation is restricted to the vegetation period in temperate and boreal regions, we apply positive net primary production (NPP) as weight to compute time-averaged stem cellulose and leaf water $\delta^{18}O$ and apply a cutoff of 1.0 g C $m^{-2}$ $month^{-1}$. This means that annual $\delta^{18}O$ of stem cellulose is calculated only based on months with a NPP higher than 1.0 g C $m^{-2}$ $month^{-1}$ and months with high NPP have a stronger weight. Effects of C storage related to the incorporation of photoassimilates from previous years into current year's cellulose is not accounted for (Gessler et al., 2007).

## 2.3 Input data

Monthly gridded meteorological data (temperature, precipitation, cloud cover, and number of wet days (CRU TS v. 3.21; Harris et al., 2014), annual atmospheric N-deposition fields (Lamarque et al., 2011), and atmospheric $CO_2$ (Etheridge et al., 1998; MacFarling Meure et al., 2006) are prescribed to LPX-Bern. The meteorological data are linearly interpolated to daily values, except for precipitation where a stochastic weather generator is applied to compute daily precipitation following Gerten et al. (2004). Monthly soil water $\delta^{18}O$, water vapor $\delta^{18}O$ and relative humidity data are from a simulation with the coupled atmosphere-land surface model ECHAM5-JSBACH for the period 1960 to 2012 (Haese et al., 2013) .

Next, the CRU climate input data are briefly evaluated. For five tree-ring sites in Switzerland (see section 2.5), we compared the CRU climate input data against relative humidity from meteorological stations (Source MeteoSwiss) and homogenized air temperature and precipitation data for Switzerland (Begert et al., 2005). For the high-elevation site at Davos (DAV) summertime (June-August, JJA) precipitation and relative humidity input data are slightly higher than data from meteorological stations in the 1960s and 70s and similar thereafter. Air temperatures for the corresponding pixel from the gridded CRU data set are around 4°C higher than in the MeteoSwiss data at DAV, as the CRU data represent averages for a large area. The

CRU data for the sites LOV and LOT compare relatively well with the meteorological station data, except for higher precipitation (both sites) and higher air temperature (site LOT).

A first-order correction is applied to the relative humidity data from ECHAM5-JSBACH to account for the daily cycle. Leaf water $^{18}O$ enrichment is driven by daytime relative humidity (when stomata are open), whereas the available ECHAM5-JSBACH data represent 24-hour averages. Relative humidity is reduced uniformly by an absolute value of 10% based on a comparison of 24-hour against 8:00-18:00 summertime average relative humidity values in temperate and boreal regions (Kearney et al., 2014). This correction was evaluated for a few summer days at the site DAV and found to be sufficient.

ECHAM5-JSBACH includes the atmosphere model ECHAM5 (Roeckner et al., 2003), and the land surface scheme JSBACH (Jena Scheme for Biosphere-Atmosphere Interaction in Hamburg; Raddatz et al., 2007). The model comprises three surface water reservoirs: a snow layer, water at the skin layer of the canopy or bare soil, and a soil water layer. These three pools are each represented by a single layer bucket model, and each of them has a prescribed maximum field capacity. In ECHAM5-JSBACH, there are no soil layers and the isotopic composition has no vertical gradient. Any water taken up by plants has the $\delta^{18}O$ of soil water. The soil layers in LPX-Bern do not affect the isotopic composition, but are exclusively used for quantitative assessment of water pools and fluxes. The drainage to groundwater in ECHAM5-JSBACH has the isotopic composition of the soil water. No fractionation during snowmelt is assumed. Liquid precipitation and melt water are added to the skin layer reservoir and the soil reservoir, respectively. After these reservoirs are filled, the residual water yields the runoff.

In order to calculate evapotranspiration in ECHAM5-JSBACH, each grid cell is divided into four cover fractions: one covered by snow, one covered with water in the skin layer reservoir, one covered by vegetation, and one covered by bare soil. The complete evapotranspiration flux is calculated by the weighted sum of these four fractions. The skin layer is modeled as a thin layer of water, which in general evaporates completely within a few model time steps.

## 2.4 Simulations

A spinup of 1500 years is performed with LPX-Bern, where an analytical solution for the C inventory in slow soil pools is applied after 1000 years to ensure that all C pools have established equilibrium conditions by the end of the spinup. Atmospheric $CO_2$ concentrations of the year 1900, atmospheric N deposition rates of 1901, climate data from 1901-1931, and $\delta^{18}O$ input data for 1960 are used during the spinup. Transient simulations are started in 1901 forced by atmospheric $CO_2$, annual N deposition (Lamarque et al., 2011), and monthly climate (see section 2.3). For the years 1901-1960 we use monthly relative humidity, soil water $\delta^{18}O$ and vapor $\delta^{18}O$ of 1960 and 1960-2012 data thereafter. All runs are for potential vegetation (no land use) and feedbacks between C and N cycles are enabled (i.e. potential limitation of growth by low N availability).

In factorial simulations, model parameters or input data are increased individually by 10% and the impact is evaluated for stem cellulose $\delta^{18}O$ for the June, July, and August 1960 average for the grid cell that includes the site DAV. In another suite of sensitivity experiments the influence of 20$^{th}$ century trends and variability on simulated $\delta^{18}O$ is explored (see section 3.3). Individual input data are kept at initial conditions, while all others are prescribed as in the standard simulation. For these sensitivity experiments monthly means of 1901-1931 are applied for air temperature, precipitation, cloud cover, and number of wet days), and monthly means of 1960-1969 for relative humidity, soil water $\delta^{18}O$ and water vapor $\delta^{18}O$, and 1901 values for atmospheric $CO_2$ and N deposition. In a similar factorial experiment, the Péclet effect is excluded. The time series are smoothed using Stineman functions. For the site DAV we carry out an additional series of experiments to evaluate the influence of a 3.5°C lower leaf than air temperature (because the 1960-2012 mean measured temperature is 3.5°C lower than the CRU temperature used in LPX-Bern), a temperature dependent biochemical fractionation as described in Sternberg and Ellsworth (2011),

$$\varepsilon_{wc} = 0.0084T^2 - 0.51T + 33.172\ , \qquad (10)$$

and this temperature dependent biochemical fractionation with measured air temperature prescribed instead of the default CRU data, while all other terms remain unchanged.

## 2.5 Tree-ring $\delta^{18}O$ data

To validate our model with regard to spatial variations, we compare mean $\delta^{18}O$ of stem cellulose for the years 1960-1996 (or until 2012 depending on availability of data) against observations from 31 sites in temperate and boreal forests (Treydte et al., 2006, 2007, 2009; Kress et al., 2010; Holzkämper et al., 2011). The sites span an area from Spain to Pakistan in the east-west and in the North-South from Morocco to Finland, but the majority is located in Europe. Measurements were performed on different tree species. In most cases, the corresponding plant functional type (temperate broad-leaved summergreen, temperate or boreal needle-leaved evergreen, or boreal needle-leaved summergreen) is simulated by LPX-Bern at the location of interest and used for model-data comparison. Otherwise, we use simulated $\delta^{18}O$ values of the dominant tree plant functional type simulated by the model. This is permissible as the differences in $\delta^{18}O$ between functional types are rather minor (see below).

Five sites in Switzerland were chosen for a comparison of time series (Table S1). DAV is a West-facing site at 1660 m above sea level (asl) dominated by the evergreen *Picea abies* (L.) H. Karst near the village of Davos. The sites on the mountain Lägern (LAEA and LAEB), situated on similar altitudes of about 720 m asl, have a South aspect, but are on different soil types. Site LAEA is on sandstone and is dominated by the deciduous broad-leaved *Fagus sylvatica* L. and the evergreen needle-leaved *Abies alba* Mill., the site LAEB is on limestone and is dominated by the two deciduous broad-leaved species *F. sylvatica* and *Fraxinus excelsior* L. However, only *F. sylvatica* is analysed here. The North-facing site in the Lötschen Valley (N19) is at 2000 m asl and is dominated by the evergreen *P. abies*. Close by is an additional site LOE in the Lötschen Valley at 2100 m asl that has a South-North exposure and is dominated by *L. decidua* (Kress et al., 2010).

For two additional sites in the Lötschen Valley at 1350 m asl and 2100 m asl (LOV, LOT), a complete set of input data at about bi-weekly resolution for the year 2008 including soil and needle water $\delta^{18}O$ for *Larix decidua* L. was available (Treydte et al., 2014). The site LOT is in immediate neighborhood to the site LOE but different trees were sampled at the two sites. In contrast to all other sites, whole wood $\delta^{18}O$ was analyzed instead of cellulose. We therefore

328 increased the whole wood values by 4.0 ‰ to convert them to cellulose, according to the constant
329 difference documented in larch for the last decades (Sidorova et al., 2008).

330 While most of these measured tree-ring $\delta^{18}O$ chronologies were derived from pooled samplings
331 of 4-5 dominant trees (Treydte et al. 2007, Kress et al. 2010), the dataset of the sites DAV,
332 LAEA, LAEB and N19 was based on measurements of individual trees, sampled within the
333 framework of the present study. Here, the sampling design covered not only dominant but also
334 smaller trees within a circular plot of about 30 m in diameter, in order to account for the full
335 range of tree ring isotopic signature within a stand (Babst et al., 2014). From about 10 trees per
336 site stable oxygen isotope ratios were measured separately for each selected tree and each year
337 over the full length of the sampled cores. Tree ring cellulose was extracted prior to measurement
338 of $\delta^{18}O$ via pyrolysis (PYRO-cube, Elementar, Hanau, Germany) and analysed for $\delta^{18}O$ by
339 isotope ratio mass spectrometry (Delta Plus XP IRMS, ThermoFinnigan MAT, Bremen,
340 Germany), as described in Weigt et al. (2015). Mean values of the individual trees per year were
341 used for site-specific $\delta^{18}O$ chronologies.

342

343 # 3 Results

344 ## 3.1 Large scale, global patterns of $\delta^{18}O$ in soil water, leaf water, and stem
345 cellulose

346 We first analyze the large scale, global patterns of $\delta^{18}O$ in soil and leaf water and in stem
347 cellulose to identify characteristic features and to evaluate the plausibility of simulated results.
348 Annual mean soil water $\delta^{18}O$ values simulated by ECHAM5-JSBACH range between -1 and -21
349 ‰ (1960-1990; Fig. 1) and are in the same range as reconstructions of $\delta^{18}O$ in precipitation from
350 the Global Network for Isotopes in Precipitation (GNIP) database (Bowen and Revenaugh, 2003).
351 For precipitation, Haease et al. (2013) estimates that the root mean square error between
352 precipitation $\delta^{18}O$ simulated by ECHAM5-JSBACH and the GNIP data is 1.78 ‰. The simulated
353 soil water $\delta^{18}O$ pattern represents major features as identified for $\delta^{18}O$ in precipitation (e.g.,
354 Bowen and Revenaugh, 2003). Namely, a decrease in $\delta^{18}O$ from mid-latitudes to high latitudes,
355 lower signatures at high elevation, and a decrease from coastal regions towards the continental

356 interior. The simulated soil water $\delta^{18}O$ pattern generally agrees with the pattern interpolated for
357 precipitation from the GNIP data (Bowen and Revenaugh, 2003).

358 Simulated leaf water $\delta^{18}O$ averaged across all plant functional types range from about -14‰ at
359 high latitudes to about 28‰ in the Middle East (Fig. 2, upper panel). Thus, the simulated $\delta^{18}O$
360 values in leaf water at the grid-cell and climatological scale span a range of ~40‰. $\delta^{18}O$ values in
361 leaf water result from the combination of soil water $\delta^{18}O$ and evaporative enrichment. There are
362 also substantial regional differences in the evaporative enrichment of $\delta^{18}O$ in leaf water mainly
363 due to large differences in air humidity, i.e. higher enrichment in arid regions than high latitude
364 regions (Fig. 3a). These differences are much larger than the differences between annual mean
365 $\delta^{18}O$ in soil water from ECHAM5-JSBACH and reconstructed $\delta^{18}O$ in precipitation discussed in
366 the previous paragraph. This suggests that soil water $\delta^{18}O$ fields from ECHAM5 provide a
367 reasonable input to force LPX-Bern simulations and that evaporative enrichment is a major
368 process shaping the spatial pattern in leaf water $\delta^{18}O$.

369 West et al. (2008) combined annual average $\delta^{18}O$ data in precipitation (Bowen and Revenaugh,
370 2003), monthly climatology for air temperature and relative humidity, and elevation data with the
371 Craig-Gordon formulation for evaporative enrichment to estimate leaf water $\delta^{18}O$. Our values
372 roughly agree with the Geographic Information System (GIS) model by West et al. (2008)(Fig. 2,
373 lower panel), but differences exist in many regions. Our estimates tend to be substantially higher
374 in e.g. Western Amazonia, Central Siberia and the Middle East, while they are significantly lower
375 for small regions in Central Africa and China. Leaf water $\delta^{18}O$ in Australia and Eastern Russia
376 agree comparatively well.

377 Differences in simulated leaf water $\delta^{18}O$ between the two approaches are much larger than
378 differences between annual mean $\delta^{18}O$ in precipitation, used by West et al. (2008) as input to
379 their GIS approach, and annual mean $\delta^{18}O$ in soil water from ECHAM5-JSBACH. Thus,
380 uncertainties in the source water input data do not explain the differences between the two
381 approaches. The mechanistic approach implemented in LPX-Bern to model leaf water isotopic
382 signatures considers seasonally varying $\delta^{18}O$ of both, source water and atmospheric water vapor,
383 and models explicitly daily stomatal conductance, transpiration, and associated $\delta^{18}O$ transport.

Tree ring cellulose $\delta^{18}O$ is in the expected range for most regions (Fig. 3b). Generally values are higher in arid regions and lower at high latitudes and range between 15 and 35‰ (Saurer et al., 2002; Ferrio and Voltas, 2005). When comparing leaf water and stem cellulose $\delta^{18}O$ with the $\delta^{18}O$ forcing used (Figs. 1, 2, 3b), it is obvious that soil water, leaf water, and cellulose $\delta^{18}O$ share a common pattern as described above. However, the simulated range of $\delta^{18}O$ in cellulose is comparable to the $\delta^{18}O$ range in soil water (or precipitation), but only half as large as the $\delta^{18}O$ range in leaf water. Due to biochemical fractionation during cellulose synthesis ($\varepsilon_{wc}$), cellulose $\delta^{18}O$ is up to 27 ‰ higher compared to leaf water $\delta^{18}O$ and cellulose depends linearly on leaf water $\delta^{18}O$. The difference between stem cellulose and leaf water $\delta^{18}O$ can be calculated by combining equations 8 and 9 and this yields a simple linear relationship with leaf water enrichment ($\delta^{18}O_{SC}$ - $\delta^{18}O_{LW}$ = $\varepsilon_{wc}$ - $p_{ex}p_x$ $\Delta^{18}O_{LW}$, where $p_{ex}p_x$ is 0.4 and $\varepsilon_{wc}$=27‰). The difference between cellulose and leaf water $\delta^{18}O$ is thus highest in regions with very low leaf water enrichment such as at high latitudes. The simulated enrichment of stem cellulose with respect to soil water is also proportional to leaf water enrichment ($\delta^{18}O_{SC}$ - $\delta^{18}O_{SW}$ = $\Delta^{18}O_{LW}$ (1-$p_{ex}p_x$) + $\varepsilon_{wc}$). The slope of this relationship is with 0.6 (1 - $p_{ex}p_x$, $p_{ex}p_x$ = 0.4) smaller than unity, which explains the smaller spatial gradients in stem cellulose $\delta^{18}O$ compared to leaf water $\delta^{18}O$.

### 3.2 Comparison of simulated stem cellulose $\delta^{18}O$ with tree ring data

Next, we quantitatively evaluate simulated $\delta^{18}O$ in stem cellulose by comparing modeled long-term (~50-yr) averages at individual grid cells with measured $\delta^{18}O$ from local, site-specific tree ring data (Table S1 in the Supplement). We recall that LPX-Bern is run with a resolution of 3.75° x 2.5° which implies mismatches between local site conditions (altitude, climate, etc.) and grid-cell averages as used to force the model. Nevertheless, simulated stem cellulose $\delta^{18}O$ agrees well with measured tree ring data from 31 sites mainly located in European temperate and boreal forests (circles in Fig. 3b, Fig. 4). The model captures the observation-based range in $\delta^{18}O$ for these sites from about 26 to 32‰ and the correlation between model and tree ring data is $r$ = 0.71 across all data points. In general the model tends to underestimate $\delta^{18}O$ values of stem cellulose. Modeled grid cell values at five Swiss sites, that will be used to explore temporal dynamics, also show somewhat lower $\delta^{18}O$ in stem cellulose (0-2‰) than the tree ring $\delta^{18}O$ data suggest (Fig. 5).

413 This holds for the alpine, high altitude sites at DAV (Fig. 5a) and in the Lötschen Valley (N19,
414 LOE, Fig. 5j,k) as well as for the low-lying sites in the Swiss Central Plateau (LAEA, LAEB,
415 Fig. 5h,i). The low bias is most strongly expressed at sites where the model is forced by very high
416 relative humidity (annual mean 1960-2012 weighted by NPP is >80%, Fig. 4 green symbols (sites
417 FON, GUT, INA, LIL, MOT)). This bias at high humidity sites could potentially arise from a bias
418 in $\delta^{18}O$ of soil water, in $\delta^{18}O$ of water vapor, or in relative humidity, and thus vapor pressure
419 deficit, and could be related to differences in the spatial scale, i.e. local measurements at
420 individual trees versus averages over all trees of a plant functional type and over a grid cell. We
421 note that daily-average relative humidity is reduced by 10% for the simulation of leaf water $\delta^{18}O$
422 to account for the lower daytime vs. 24-hour humidity; uncertainties in this correction have a
423 larger influence on the water vapor pressure deficit, the driving force for transpiration, at humid
424 sites. At a single site (CAZ) where LPX-Bern simulates extremely low biomass of less than 30 g
425 C $m^{-2}$, because herbaceous plants dominate in this grid cell, stem cellulose $\delta^{18}O$ is also
426 underestimated (open symbol in Fig. 4). Excluding this site and the very humid sites yields a
427 correlation coefficient of $r = 0.65$, which is not higher than for all sites. We conclude that LPX-
428 Bern is able to represent the magnitude and the spatial climatological pattern of $\delta^{18}O$ in stem
429 cellulose in Europe, generally within a few per mil of available observations.

430

431 This conclusion is further corroborated by comparing LPX-Bern results with $\delta^{18}O$ data from two
432 Swiss sites (LOV, LOT) for which detailed $\delta^{18}O$ data are available for soil water, needle water,
433 and stem wood (Table 1), but for a single year only. Simulated enrichment of needle water above
434 soil water as well as simulated enrichment of stem cellulose above needle water is within the
435 observed range at the two sites (Table 1). We note that this comparison is somewhat hampered by
436 the large variability in the weekly samples (e.g., for leaf water $\delta^{18}O$ at LOV: 3.9-16.4‰ and at
437 LOT: -4.6-11.4‰) that LPX-Bern cannot reproduce because the model is driven by monthly data.

438 The inter-annual variability and decadal-scale trends of stem cellulose $\delta^{18}O$ are analyzed for five
439 tree ring sites in Switzerland and for the period 1960 to 2012 for which temporally resolved input
440 data from ECHAM5-JSBACH are available (Fig. 5). Due to the coarse spatial resolution of the
441 gridded LPX-Bern version applied here, all sites except DAV lie within the same grid cell and
442 model results are almost identical. Slight differences in the model time series shown in Figure 5

443 are due to differences in tree functional types (LAEA/LAEB: deciduous broad-leaved, N19:
444 evergreen needle-leaved, LOE: deciduous needle-leaved; thin lines in Fig. 5h-k) selected for the
445 comparison with the tree ring $\delta^{18}O$ data.

446 The simulated stem cellulose $\delta^{18}O$ time series capture the measured evolution and inter-annual
447 variability (Fig. 5a,h-k). Based on visual comparison, the correlation between simulated and
448 measured stem cellulose $\delta^{18}O$ is best in the 60s and early 70s and is weaker thereafter. Model
449 values increase after 1990 probably due to higher temperature and soil water $\delta^{18}O$, which is not
450 recognized in the tree ring data. For the entire time series the correlations range between 0.48 and
451 0.73, with the highest value at LAEA in the Swiss central plateau (Fig. 5h) and the lowest value
452 at the alpine site DAV (Fig. 5a). The correlation coefficients are comparable to the correlations
453 between the four tree ring series in the Swiss Central Plateau (LAEA, LAEB) and the Lötschen
454 Valley (N19, LOE) which range between 0.55 and 0.82. In other words, the correlation between
455 measured and modeled grid cell values reflects site-to-site variability within the grid-cell. In
456 conclusion, not only the reconstructed climatological mean pattern across Europe, but also the
457 reconstructed temporal variability in stem cellulose $\delta^{18}O$ at individual Swiss sites is generally
458 well represented by LPX-Bern.

459

460 An extreme heat wave hit Europe in 2003 (Figs. 5, 7, S2, and S3) with summer temperatures of
461 3°C above the 1961 to 1990 mean (Schär et al., 2004) and one expects to find extreme values in
462 $\delta^{18}O$. Indeed, simulated stem cellulose $\delta^{18}O$ peaks in this year with record or near-record high
463 values for the analysis period (Fig. 5). Very low humidity and high air temperatures most likely
464 lead to strong leaf water $\delta^{18}O$ enrichment. Surprisingly, the response in $\delta^{18}O$ in the tree ring data
465 is different for different sites. Measurements at LAEA, N19, and LOE show a strong peak in $\delta^{18}O$
466 (Fig. 5h,j,k), DAV a small peak (Fig. 5a), and site LAEB even lower values than during the
467 previous and following year (Fig. 5i). Apparently, local differences in conditions or different
468 reactions of different tree species may mask the expected drought signal in stem cellulose $\delta^{18}O$. A
469 well-known phenomenon is that extreme conditions may not be captured because growth is
470 stopped and the signal therefore not recorded (Sarris et al. 2013).

471

### 3.3 Sensitivity analysis to explore the influence of individual drivers

Simulated variability in stem cellulose $\delta^{18}O$ arises from various drivers and their influence is quantified within LPX-Bern. In the standard simulation with the combination of all drivers, air temperature, soil water $\delta^{18}O$ and water vapor $\delta^{18}O$ are positively correlated with cellulose $\delta^{18}O$ as demonstrated for site DAV (Fig. 5b,d,e). In contrast, relative humidity and precipitation are negatively correlated with cellulose $\delta^{18}O$ (Fig. 5c,f). The correlation is strongest with soil water $\delta^{18}O$ suggesting a high dependence of our results on the isotope input data.

The influence of various drivers on cellulose $\delta^{18}O$ is further investigated in transient factorial simulations where individual drivers were kept at their climatological mean values representative for the early 20$^{th}$ century for the meteorological variables temperature, precipitation, cloud cover, and number of wet days, and 1960 values for relative humidity, $\delta^{18}O$ soil water and water vapor input data. The results (Fig. 6) show that, in order of importance, variations in relative humidity, temperature, $\delta^{18}O$ in soil water, and water vapor $\delta^{18}O$ force decadal-scale and inter-annual variability in cellulose $\delta^{18}O$. The simple sensitivity analysis for the site DAV, where input data or parameters were increased by 10%, also reveals that stem cellulose $\delta^{18}O$ is sensitive to changes in relative humidity, soil water and water vapor $\delta^{18}O$ (Table 2). Precipitation had no influence on stem cellulose $\delta^{18}O$ in the transient simulation (Fig. 6a). In contrast, accounting for the Péclet effect, resulted in consistently lower values with nearly no influence on inter-annual variation (Fig. 6b). Atmospheric $CO_2$ had a very minor effect on cellulose $\delta^{18}O$ (<0.04‰ except for a single year with an effect of 0.18‰), while N deposition had no influence (Fig. 6b). In years when relative humidity and temperature had a positive effect, the combined effect of temperature, precipitation, number of wet days and cloud cover (termed "clim effect" in Fig. 6a) was often large and also positive. In years when the influence of relative humidity and temperature had opposing signs, the clim effect was around zero. The 20$^{th}$ century trends in air temperature mostly led to higher stem cellulose $\delta^{18}O$ during the last five decades compared to the early 20$^{th}$ century. The clim effect leads to slightly higher decadal-averaged values in stem cellulose $\delta^{18}O$ (+0-2‰) towards the end of the simulation. However, these values are not unusual in the context of the decadal variability simulated for the past five decades.

501 Sensitivities of cellulose $\delta^{18}O$ to the input data are similar at all sites (Fig. 6c-e). Compared to
502 DAV, the magnitude of the decadal-scale trends induced by "climate" and soil water $\delta^{18}O$
503 changes are somewhat smaller at other sites though. Conversely, changes in relative humidity
504 have a stronger influence at LAEB and N19. At all sites, the prescribed changes in relative
505 humidity (i.e. keeping values at mean representative for the early 20$^{th}$ century) cause on average
506 lower cellulose $\delta^{18}O$ during the 1980s than compared to the end of the simulation. Decadal-scale
507 variability is also related to changes in soil water $\delta^{18}O$. In particular, soil water $\delta^{18}O$ variations
508 caused an increase in stem cellulose $\delta^{18}O$ of about 0.3 to 0.5 ‰ in the 1980s that persisted
509 thereafter (Fig. 6e). A similar trend was simulated for "climate", but with more variability
510 between sites. At N19 the "climate" effect was always lowest and there was no clear trend. In
511 brief, LPX-Bern simulates substantial inter-annual and decadal scale variability in stem cellulose
512 $\delta^{18}O$ which is attributable to variability in relative humidity, temperature, and $\delta^{18}O$ in soil water
513 and vapor.

514

515 West et al. (2008) assumed that leaf temperature exceeds air temperature by 5°C in their
516 implementation of the Craig-Gordon model. Since CRU air temperatures are on average 3.5°C
517 higher than measured temperatures for the Swiss site DAV (Fig. 7), we did not want to further
518 increase them. Instead we tested the effect of reducing leaf temperature by 3.5°C compared to air
519 temperature, which improved the correlation of simulated and measured stem cellulose $\delta^{18}O$ at
520 DAV and increased the simulated stem cellulose $\delta^{18}O$ compared to the original simulation (Fig. 8,
521 'Tleaf' vs. 'LPX-Bern standard simulation': 27.05‰ vs. 26.47‰ (average for 1960-2012)).
522 Similarly, accounting for a temperature dependent biochemical fractionation ('ewcT') led to
523 consistently higher cellulose $\delta^{18}O$ (27.21‰) compared to the standard simulation, with a nearly
524 identical correlation coefficient compared to the 'Tleaf' simulation. When the temperature-
525 dependent formulation for $\varepsilon_{wc}$ was combined with temperature forcing from a nearby
526 meteorological station ('ewcTmeteo'), stem cellulose $\delta^{18}O$ increased further and was even slightly
527 higher than the measured data (28.47‰ vs. 28.02‰, average for 1960-2012). The correlation
528 remained equally good though compared to the simulation with a temperature dependent $\varepsilon_{wc}$ and
529 CRU climate. We also evaluated temporal mean stem cellulose across all (European) sites.
530 Compared to the original simulations (Fig. 4) the correlation between modeled and measured data

was slightly lower if $\varepsilon_{wc}$ was allowed to depend on temperature ($r$ = 0.68 vs. $r$ = 0.71, data not shown). Since we know that the CRU temperatures are too low for some sites (e.g. Fig. 7), we performed an additional test where we set $\varepsilon_{wc}$ to 31‰ to mimic the effect of low growth temperatures on biochemical fractionation. This test should improve results for cool sites (INA, GUT, ILO, CAV), which was indeed what we observed. For these sites the model-observation differences decreased (results not shown), while for sites with high mean annual temperatures (e.g. REN, LIL) LPX-Bern overestimated stem cellulose $\delta^{18}O$ or left them unchanged.

## 4 Discussion and Conclusion

Formulations to describe $\delta^{18}O$ in leaf water and stem cellulose are implemented in the LPX-Bern DGVM and a compilation of tree ring data of $\delta^{18}O$ in stem cellulose, mainly for Europe, is established. This allows us to model the large scale distribution of leaf water and stem cellulose $\delta^{18}O$ on the global scale, to study spatio-temporal variability in $\delta^{18}O$, to evaluate model formulations describing the transfer of $\delta^{18}O$ signals within plants, and, last but not least, to investigate underlying drivers and processes. Further, the model permits us to address how inter-annual, decadal and 20$^{th}$ century changes in climate and environmental variables may have affected $\delta^{18}O$ in stem cellulose, thereby contributing to the interpretation of tree ring $\delta^{18}O$ data.

The comparison of 50-yr-averaged model results with tree ring data, mainly across Europe, shows that the large scale climatological-mean pattern in stem cellulose $\delta^{18}O$ is well captured by the model (Fig. 4). The high correlation between modeled time series and $\delta^{18}O$ tree ring data from five sites in Switzerland suggests that the inter-annual variability in stem cellulose $\delta^{18}O$ is also well represented by LPX-Bern (Fig. 5). Thus, the formulations describing water uptake by plants and transpiration, regulated by stomatal conductance and influenced by ambient $CO_2$ concentrations, and corresponding isotope fractionations appear consistent with tree ring $\delta^{18}O$ data. In an earlier study (Saurer et al., 2014), it is shown that LPX-Bern is also able to represent the spatial gradients in $\delta^{13}C$ and the temporal change in $\delta^{13}C$ and intrinsic water use efficiency over the 20$^{th}$ century as reconstructed from a European-wide tree ring network. The good agreement with tree ring data suggests that LPX-Bern is suited to explore the $\delta^{18}O$ signal transfer

560 within forest ecosystems and to study the relationship between $\delta^{18}O$ in stem cellulose and
561 meteorological drivers in a mechanistic way, at least within European boreal and temperate
562 forests. This aspect may become particularly relevant in the context of global warming, with
563 more extreme conditions including heat waves and droughts expected. The model could be used
564 in future work in connection with tree ring data of growth, $\delta^{13}C$, and $\delta^{18}O$ to study the nexus
565 between flows of water (governing evaporative cooling and runoff) and C as well as C
566 sequestration. In general, we expect any changes in seasonality that could potentially affect soil
567 water $\delta^{18}O$ such as e.g. earlier snow melt to be translated to stem cellulose $\delta^{18}O$ in LPX-Bern.
568
569 Inter-annual variability and decadal scale trends of modeled tree-ring $\delta^{18}O$ in Switzerland are
570 predominantly driven by the meteorological variables relative humidity and temperature and the
571 variability in soil water and water vapor $\delta^{18}O$ (Fig. 6, Table 2). In contrast, N deposition or
572 increasing $CO_2$ leading to $CO_2$ fertilization within LPX-Bern do not influence trends and
573 variability in stem cellulose $\delta^{18}O$ at the investigated sites. This is a novel finding that is important
574 for tree-ring $\delta^{18}O$ interpretation, and contrasts with respective findings for $\delta^{13}C$, where $CO_2$ is an
575 important factor (Saurer et al. 2014). A strong influence of relative humidity and soil water on
576 stem cellulose $\delta^{18}O$ is consistent with expectations from isotope theory (McCarroll and Loader,
577 2004). This is also in agreement with many tree-ring studies that found a significant effect of
578 relative humidity (Burk and Stuiver, 1981), vapor pressure differences (Kahmen et al., 2011) and
579 $\delta^{18}O$ of precipitation (Waterhouse et al., 2002) based on statistical analyses. Precipitation
580 variations in our study did not influence inter-annual variability nor long-term trends in stem
581 cellulose $\delta^{18}O$ in factorial simulations where precipitation is kept constant at climatological mean
582 values. Hence, it seems unlikely that $\delta^{18}O$ as simulated by LPX-Bern will capture changes in
583 precipitation patterns that are not associated with changes in isotope signals. Nevertheless, time
584 series of precipitation at DAV are correlated with modeled time series of $\delta^{18}O$ in stem cellulose
585 (Fig. 5c) in agreement with observations (e.g. Reynolds-Henne et al., 2007; Rinne et al., 2013;
586 Hartl-Meier et al., 2015), albeit less than correlations for soil and water vapor $\delta^{18}O$ (Fig. 5b,d), air
587 temperature and humidity (Fig. 5e,f). This correlation likely arises from the impact of
588 precipitation on other variables, e.g. relative humidity, and from the correlation of precipitation
589 with other driving variables. There is clearly decadal variability in simulated stem cellulose $\delta^{18}O$

590 linked to variability in $\delta^{18}O$ and climate input data, e.g. the effect of soil water $\delta^{18}O$ varied around
591 zero in the 1960s and is consistently positive in the 1990s (Fig. 6e).The identification of potential
592 century-scale trends is hampered by the lack of suitable input data for relative humidity and $\delta^{18}O$
593 of soil water and water vapor in this study.

594 There are several sources of uncertainty that may explain the remaining deviations between
595 simulated and measured stem cellulose $\delta^{18}O$ for the Swiss and European sites. First, we run the
596 model at a coarse spatial resolution (about 220 km x 320 km in Southern Europe) and local site
597 conditions are expected to be different from grid cell average conditions. Climate input data and
598 prescribed $\delta^{18}O$ in soil water and water vapor therefore only approximate local values at the site.
599 Sensitivity simulations (Table 2) and a comparison of soil water $\delta^{18}O$ with the $\delta^{18}O$ from the
600 GNIP precipitation network reveal that uncertainties in the input data can indeed well explain
601 deviations between modeled and measured $\delta^{18}O$ in stem cellulose. Uncertainties in relative
602 humidity appear particularly relevant and are likely at the origin of relatively large data-model
603 discrepancies at humid sites. Only modest changes in humidity, and thus water pressure deficit,
604 do result in significant changes in stem cellulose $\delta^{18}O$. Daily variations and within canopy
605 variations in humidity (and other variables) are not taken into account in our approach. Second,
606 we assume that parameters such as the fractionation between water and cellulose, $\varepsilon_{wc}$, the path
607 length, $L$, for the Péclet effect or the proportion of carbonyl oxygen exchange with source water,
608 $p_{ex}$, are constant, although they may vary (e.g. Wang et al., 1998; Ripullone et al., 2008;
609 Sternberg and Ellsworth, 2011; Song et al., 2014). The biochemical fractionation factor $\varepsilon_{wc}$ is
610 commonly assumed to be 27‰. Only recently Sternberg & Ellsworth (2011) suggested that $\varepsilon_{wc}$
611 increases up to about 31‰ at low growth temperatures of 5°C. However, their experiments were
612 performed in a rather artificial system as they studied wheat seedlings cultivated in the dark and
613 their findings are controversially discussed (Sternberg, 2014; Zech et al., 2014). Application of a
614 temperature dependent $\varepsilon_{wc}$ in LPX-Bern in combination with meteorological data from a nearby
615 weather station removed the model-measurement offset for the alpine site DAV and improved the
616 model-measurement correlation compared to the standard setup. So far our results seem the first
617 to indicate that a temperature dependent $\varepsilon_{wc}$ might perhaps also be relevant under field conditions.
618 Yet, uncertainties in other input data and model structure are too large to draw any firm
619 conclusions. The path length ($L$) of 0.03 m for the Péclet number agrees with previous studies

(Wang et al., 1998; Gessler et al., 2013), although large variability has been reported (Kahmen et al., 2009). Also the proportion of carbonyl oxygen exchange with source water ($p_{ex}$) of 0.4 seems reasonable compared with published values (Cernusak et al., 2005; Gessler et al., 2009; Gessler et al., 2013; Song et al., 2014). However, relatively small changes in $p_{ex}$ have a significant impact on $\delta^{18}O$ in stem cellulose (Table 2) and recent studies suggest this value could range between 0.2 and 0.42 (Gessler et al., 2009; Song et al., 2014). Third, in LPX-Bern, photoassimilates are allocated to growing tissues instantaneously and are not stored e.g. as starch. The simulated tree ring $\delta^{18}O$ is therefore exclusively affected by the current year's meteorology, and not by that of previous years.

The fact that soil water $\delta^{18}O$ has a strong effect on stem cellulose $\delta^{18}O$ calls for a very careful evaluation of the source water input data. Unfortunately oxygen isotope ratios of soil water are not systematically measured as is the case for precipitation (Global Network for Isotopes in Precipitation, The GNIP Database, http://www.iaea.org/water). However, the comparison of the soil water $\delta^{18}O$ data from the ECHAM5-JSBACH model as used as input to LPX-Bern with the GNIP data reveal a good agreement and deviations in $\delta^{18}O$ between ECHAM5-JSBACH soil and GNIP precipitation $\delta^{18}O$ data are generally less than two per mill (Haese et al. 2013).

Our leaf water $\delta^{18}O$ results provide another global scale estimate of leaf water $\delta^{18}O$ in addition to the GIS-based approach by West et al. (2008). There are several possible reasons that could explain why leaf water $\delta^{18}O$ simulated by LPX-Bern was mostly higher compared to simulations by West et al. (2008) (Fig. 2). First, the $\delta^{18}O$ input data and relative humidity forcings were not the same. West and colleagues used annually-averaged $\delta^{18}O$ from the GNIP precipitation network, which obviously provides lower values than when summer $\delta^{18}O$ would have been used. The mechanistic approach implemented in LPX-Bern considers seasonally varying $\delta^{18}O$ of both, source water and atmospheric water vapor, and models explicitly daily stomatal conductance, transpiration, and associated $\delta^{18}O$ transport. Second, West et al. (2008) assumed that leaf temperature is 5°C higher than air temperature. Observations support this for broad-leaved, but less so for needle leaved species (Leuzinger and Körner, 2007). Because sites with conifers dominate our observational data set, it is reasonable to assume that leaf temperature equals air temperature in our study. We only have few measurements to support this and more field data would be needed for a meaningful evaluation of simulated leaf water $\delta^{18}O$. Nevertheless, the

LPX-Bern simulated mean value of leaf water $\delta^{18}O$ for one grid cell is within the range of the mean values measured at two sites in this grid cell (Table 1). Additionally, the good agreement between measured and modeled stem cellulose $\delta^{18}O$ in Europe appears to implicitly support the LPX-Bern estimates in leaf water $\delta^{18}O$ for this region.

We implemented routines to simulate leaf water and stem cellulose $\delta^{18}O$ in the LPX-Bern DGVM and successfully modeled the spatio-temporal variability in $\delta^{18}O$ as revealed by European tree ring data. As tree-ring isotope networks are becoming more wide-spread, the $^{18}O$-enabled LPX-Bern model provides an ideal tool to explore large-scale spatial and temporal patterns in cellulose $\delta^{18}O$ and to help unravel underlying processes and drivers.

## Acknowledgements

We thank Martin Werner for providing the soil water and humidity $\delta^{18}O$ data from the ECHAM5-JSBACH model, and Kerstin Treydte for sharing data from two of the Lötschen Valley sites. Jason West is acknowledged for providing the leaf water $\delta^{18}O$ data and Ansgar Kahmen for sharing his offline model. We thank Rolf Siegwolf for his valuable input and Raphael Roth for support during model development. Measurements from weather stations are from MeteoSwiss, the Swiss Federal Office of Meteorology and Climatology. This study is supported by the Swiss National Science Foundation (SNF) through the Sinergia Project iTREE (CRSII3_136295) and the grant to the Division of Climate and Environmental Physics (200020-14174).

673 **References**


674 An, W., Liu, X., Leavitt, S. W., Xu, G., Zeng, X., Wang, W., Qin, D., and Ren, J.: Relative
675 humidity history on the Batang-Litang Plateau of western China since 1755 reconstructed from
676 tree-ring $\delta^{18}O$- and $\delta$ D, Climate Dynamics, 42, 2639-2654, 2014.

677 Anderson, W. T., Bernasconi, S. M., McKenzie, J. A., and Saurer, M.: Oxygen and carbon
678 isotopic record of climatic variability in tree ring cellulose (*Picea abies*): An example from
679 central Switzerland (1913-1995), Journal of Geophysical Research-Atmospheres, 103, 31625-
680 31636, 1998.

681 Babst, F., Alexander, M. R., Szejner, P., Bouriaud, O., Klesse, S., Roden, J., Ciais, P., Poulter, B.,
682 Frank, D., Moore, D. J. P., and Trouet, V.: A tree-ring perspective on the terrestrial carbon cycle,
683 Oecologia, 176, 307-322, 10.1007/s00442-014-3031-6, 2014.

684 Barbour, M. M., and Farquhar, G. D.: Relative humidity- and ABA-induced variation in carbon
685 and oxygen isotope ratios of cotton leaves, Plant Cell and Environment, 23, 473-485, 2000.

686 Barbour, M. M., Roden, J. S., Farquhar, G. D., and Ehleringer, J. R.: Expressing leaf water and
687 cellulose oxygen isotope ratios as enrichment above source water reveals evidence of a Péclet
688 effect, Oecologia, 138, 426-435, 2004.

689 Barbour, M. M.: Stable oxygen isotope composition of plant tissue: a review, Functional Plant
690 Biology, 34, 83-94, http://dx.doi.org/10.1071/FP06228, 2007.

691 Begert, M., Schlegel, T., and Kirchhofer, W.: Homogeneous temperature and precipitation series
692 of Switzerland from 1864 to 2000, International Journal of Climatology, 25, 65-80,
693 doi/10.1002/joc.1118/abstract, 2005.

694 Bottinga, Y., and Craig, H.: Oxygen isotope fractionation between $CO_2$ and water and isotopic
695 composition of marine atmospheric $CO_2$, Earth and Planetary Science Letters, 5, 285-295, 1969.

696 Bowen, G. J., and Revenaugh, J.: Interpolating the isotopic composition of modern meteoric
697 precipitation, Water Resources Research, 39, 1299, 2003.

698 Burk, R. L., and Stuiver, M.: Oxygen isotope ratios in trees reflect mean annual temperature and
699 humidity, Science, 211, 1417-1419, 1981.

700 Cappa, C. D., Hendricks, M. B., DePaolo, D. J., and Cohen, R. C.: Isotopic fractionation of water
701 during evaporation, Journal of Geophysical Research: Atmospheres, 108, 1-10,
702 10.1029/2003jd003597, 2003.

703 Cernusak, L. A., Farquhar, G. D., and Pate, J. S.: Environmental and physiological controls over
704 oxygen and carbon isotope composition of Tasmanian blue gum, *Eucalyptus globulus*, Tree
705 Physiology, 25, 129-146, 2005.

706 Collatz, G. J., Ball, J. T., Grivet, C., and Berry, J. A.: Physiological and environmental regulation
707 of stomatal conductance, photosynthesis and transpiration - A model that includes a laminar
708 boundary layer, Agricultural and Forest Meteorology, 54, 107-136, 1991.

709 Collatz, G. J., Ribas-Carbo, M., and Berry, J. A.: Coupled photosynthesis-stomatal conductance
710 model for leaves of $C_4$ plants, Australian Journal of Plant Physiology, 19, 519-538, 1992.

711 Craig, H., and Gordon, L.: Deuterium and oxygen 18 variations in the ocean and the marine
712 atmosphere, Consiglio Nazionale delle Ricerche, Laboratorio di Geologia Nucleare, Pisa, 1965.

713 Cuntz, M., Ogée, J., Farquhar, G. D., Peylin, P., and Cernusak, L. A.: Modelling advection and
714 diffusion of water isotopologues in leaves, Plant, Cell & Environment, 30, 892-909,
715 10.1111/j.1365-3040.2007.01676.x, 2007.

716 Dansgaard, W.: Stable isotopes in precipitation, Tellus A, 16, 10.3402/tellusa.v16i4.8993, 1964.

717 Dongmann, G., Nürnberg, H. W., Förstel, H., and Wagener, K.: On the enrichment of $H_2{}^{18}O$ in
718 the leaves of transpiring plants, Radiation and Environmental Biophysics, 11, 41-52,
719 10.1007/BF01323099, 1974.

720 Dunbar, R. B., Wellington, G. M., Colgan, M. W., and Glynn, P. W.: Eastern Pacific sea-surface
721 temperature since 1600 A.D.: The $\delta^{18}O$ record of climate variability in Galápagos corals,
722 Paleoceanography, 9, 291-315, 1994.

723 Edwards, T. W. D., Birks, S. J., Luckman, B. H., and MacDonald, G. M.: Climatic and
724 hydrologic variability during the past millennium in the eastern Rocky Mountains and northern
725 Great Plains of western Canada, Quaternary Research, 70, 188-197,
726 dx.doi.org/10.1016/j.yqres.2008.04.013, 2008.

727 Elderfield, H., and Ganssen, G.: Past temperature and $\delta^{18}O$ of surface ocean waters inferred from
728 foraminiferal Mg/Ca ratios, Nature, 405, 442-445, 2000.

729 Epstein, S., Thompson, P., and Yapp, C. J.: Oxygen and hydrogen isotopic ratios in plant
730 cellulose, Science, 198, 1209-1215, 1977.

731 Etheridge, D. M., Steele, L. P., Langenfelds, R. L., Francey, R. J., Barnola, J. M., and Morgan, V.
732 I.: Historical $CO_2$ records from the Law Dome DE08, DE08-2, and DSS ice cores, in: Trends: A
733 Compendium of Data on Global Change. Carbon Dioxide Information Analysis Center, Oak
734 Ridge National Laboratory, U.S. Department of Energy
735 http://cdiac.ornl.gov/trends/co2/lawdome.html, Oak Ridge, Tenn., U.S.A, 1998.

736 Farquhar, G. D., von Caemmerer, S., and Berry, J. A.: A biochemical model of photosynthetic
737 $CO_2$ assimilation in leaves of $C_3$ species, Planta, 149, 78-90, 1980.

738 Farquhar, G. D., and von Caemmerer, S.: Modelling of photosynthetic response to environmental
739 conditions, in: Physiological Plant Ecology II: Water Relations and Carbon Assimilation, edited
740 by: Nobel, P. S., Osmond, C. B., and Ziegler, H., Spriner, Berlin, 549-587, 1982.

741 Farquhar, G. D., and Lloyd, J.: Carbon and oxygen isotope effects in the exchange of carbon
742 dioxide between terrestrial plants and the atmosphere., in: Stable isotopes and plant carbon–water
743 relations, edited by: Ehleringer, J. R., Hall, A. E., and Farquhar, G. D., Academic Press, San
744 Diego, 47–70, 1993.

745 Farquhar, G. D., and Gan, K. S.: On the progressive enrichment of the oxygen isotopic
746 composition of water along a leaf, Plant Cell and Environment, 26, 1579-1597, 2003.

747 Ferrio, J. P., and Voltas, J.: Carbon and oxygen isotope ratios in wood constituents of *Pinus*
748 *halepensis* as indicators of precipitation, temperature and vapour pressure deficit, Tellus Series B-
749 Chemical and Physical Meteorology, 57, 164-173, 2005.

Flanagan, L. B., Comstock, J. P., and Ehleringer, J. R.: Comparison of Modeled and Observed Environmental Influences on the Stable Oxygen and Hydrogen Isotope Composition of Leaf Water in *Phaseolus vulgaris* L., Plant Physiology, 96, 588-596, 1991.

Fleitmann, D., Burns, S. J., Neff, U., Mudelsee, M., Mangini, A., and Matter, A.: Palaeoclimatic interpretation of high-resolution oxygen isotope profiles derived from annually laminated speleothems from Southern Oman, Quaternary Science Reviews, 23, 935-945, 10.1016/j.quascirev.2003.06.019, 2004.

Gerten, D., Schaphoff, S., Haberlandt, U., Lucht, W., and Sitch, S.: Terrestrial vegetation and water balance - hydrological evaluation of a dynamic global vegetation model, Journal of Hydrology, 286, 249-270, 2004.

Gessler, A., Keitel, C., Kodama, N., Weston, C., Winters, A. J., Keith, H., Grice, K., Leuning, R., and Farquhar, G. D.: $\delta^{13}C$ of organic matter transported from the leaves to the roots in *Eucalyptus delegatensis*: short-term variations and relation to respired $CO_2$, Functional Plant Biology, 34, 692-706, 10.1071/fp07064, 2007.

Gessler, A., Brandes, E., Buchmann, N., Helle, G., Rennenberg, H., and Barnard, R. L.: Tracing carbon and oxygen isotope signals from newly assimilated sugars in the leaves to the tree-ring archive, Plant Cell and Environment, 32, 780-795, 2009.

Gessler, A., Brandes, E., Keitel, C., Boda, S., Kayler, Z. E., Granier, A., Barbour, M., Farquhar, G. D., and Treydte, K.: The oxygen isotope enrichment of leaf-exported assimilates - does it always reflect lamina leaf water enrichment?, New Phytologist, 200, 144-157, 2013.

Gessler, A., Pedro Ferrio, J., Hommel, R., Treydte, K., Werner, R. A., and Monson, R. K.: Stable isotopes in tree rings: towards a mechanistic understanding of isotope fractionation and mixing processes from the leaves to the wood, Tree Physiology, 34, 796-818, 2014.

Haese, B., Werner, M., and Lohmann, G.: Stable water isotopes in the coupled atmosphere–land surface model ECHAM5-JSBACH, Geosci. Model Dev., 6, 1463-1480, 10.5194/gmd-6-1463-2013, 2013.

Harris, I., Jones, P. D., Osborn, T. J., and Lister, D. H.: Updated high-resolution grids of monthly climatic observations - the CRU TS3.10 Dataset, International Journal of Climatology, 34, 623-642, 2014.

Hartl-Meier, C., Zang, C., Buentgen, U., Esper, J., Rothe, A., Goettlein, A., Dirnboeck, T., and Treydte, K.: Uniform climate sensitivity in tree-ring stable isotopes across species and sites in a mid-latitude temperate forest, Tree Physiology, 35, 4-15, 2015.

Haxeltine, A., and Prentice, I. C.: A general model for the light-use efficiency of primary production, Functional Ecology, 10, 551-561, 1996a.

Haxeltine, A., and Prentice, I. C.: BIOME3: An equilibrium terrestrial biosphere model based on ecophysiological constraints, resource availability, and competition among plant functional types, Global Biogeochemical Cycles, 10, 693-709, 1996b.

Herweijer, C., Seager, R., Cook, E. R., and Emile-Geay, J.: North American droughts of the last millennium from a gridded network of tree-ring data, Journal of Climate, 20, 1353-1376, 2007.

789 Hoffmann, G., Werner, M., and Heimann, M.: Water isotope module of the ECHAM atmospheric
790 general circulation model: A study on timescales from days to several years, Journal of
791 Geophysical Research-Atmospheres, 103, 16871-16896, 1998.

792 Hoffmann, G., Ramirez, E., Taupin, J. D., Francou, B., Ribstein, P., Delmas, R., Durr, H.,
793 Gallaire, R., Simoes, J., Schotterer, U., Stievenard, M., and Werner, M.: Coherent isotope history
794 of Andean ice cores over the last century, Geophysical Research Letters, 30, 1179, 2003.

795 Johnsen, S. J., Dahl-Jensen, D., Gundestrup, N., Steffensen, J. P., Clausen, H. B., Miller, H.,
796 Masson-Delmotte, V., Sveinbjörnsdottir, A. E., and White, J.: Oxygen isotope and
797 palaeotemperature records from six Greenland ice-core stations: Camp Century, Dye-3, GRIP,
798 GISP2, Renland and NorthGRIP, Journal of Quaternary Science, 16, 299-307, 10.1002/jqs.622,
799 2001.

800 Joussaume, S., Sadourny, R., and Jouzel, J.: A general circulation model of water isotope cycles
801 in the atmosphere, Nature, 311, 24-29, 1984.

802 Jouzel, J., Russell, G. L., Suozzo, R. J., Koster, R. D., White, J. W. C., and Broecker, W. S.:
803 Simulations of the HDO and $H_2O^{18}$ atmospheric cycles using the NASA GISS general-circulation
804 model - The seasonal cycle for present-day conditions, Journal of Geophysical Research-
805 Atmospheres, 92, 14739-14760, 1987.

806 Jouzel, J., Vimeux, F., Caillon, N., Delaygue, G., Hoffmann, G., Masson-Delmotte, V., and
807 Parrenin, F.: Magnitude of isotope/temperature scaling for interpretation of central Antarctic ice
808 cores, Journal of Geophysical Research-Atmospheres, 108, 4361, 2003.

809 Kahmen, A., Simonin, K., Tu, K., Goldsmith, G. R., and Dawson, T. E.: The influence of species
810 and growing conditions on the 18-O enrichment of leaf water and its impact on 'effective path
811 length', New Phytologist, 184, 619-630, 10.1111/j.1469-8137.2009.03008.x, 2009.

812 Kahmen, A., Sachse, D., Arndt, S. K., Tu, K. P., Farrington, H., Vitousek, P. M., and Dawson, T.
813 E.: Cellulose $\delta^{18}O$ is an index of leaf-to-air vapor pressure difference (VPD) in tropical plants,
814 Proceedings of the National Academy of Sciences of the United States of America, 108, 1981-
815 1986, 10.1073/pnas.1018906108, 2011.

816 Kearney, M. R., Isaac, A. P., and Porter, W. P.: microclim: Global estimates of hourly
817 microclimate based on long-term monthly climate averages, Scientific Data, 1, 2014.

818 Kern, Z., Kohan, B., and Leuenberger, M.: Precipitation isoscape of high reliefs: interpolation
819 scheme designed and tested for monthly resolved precipitation oxygen isotope records of an
820 Alpine domain, Atmospheric chemistry and physics, 14, 1897-1907, 2014.

821 Kress, A., Saurer, M., Siegwolf, R. T. W., Frank, D. C., Esper, J., and Bugmann, H.: A 350 year
822 drought reconstruction from Alpine tree ring stable isotopes, Global Biogeochemical Cycles, 24,
823 GB2011, 2010.

824 Lamarque, J.-F., Kyle, G. P., Meinshausen, M., Riahi, K., Smith, S. J., van Vuuren, D. P.,
825 Conley, A. J., and Vitt, F.: Global and regional evolution of short-lived radiatively-active gases
826 and aerosols in the Representative Concentration Pathways, Climatic Change, 109, 191-212,
827 2011.

Leuzinger, S., and Körner, C.: Tree species diversity affects canopy leaf temperatures in a mature temperate forest, Agricultural and Forest Meteorology, 146, 29-37, 2007.

Libby, L. M., Pandolfi, L. J., Payton, P. H., Marshall, J., Becker, B., and Giertz-Sienbenlist, V.: Isotopic tree thermometers, Nature, 261, 284-288, 10.1038/261284a0, 1976.

MacFarling Meure, C., Etheridge, D., Trudinger, C., Steele, P., Langenfelds, R., van Ommen, T., Smith, A., and Elkins, J.: Law Dome $CO_2$, $CH_4$ and $N_2O$ ice core records extended to 2000 years BP, Geophysical Research Letters, 33, L14810, 2006.

Masson-Delmotte, V., Raffalli-Delerce, G., Danis, P. A., Yiou, P., Stievenard, M., Guibal, F., Mestre, O., Bernard, V., Goosse, H., Hoffmann, G., and Jouzel, J.: Changes in European precipitation seasonality and in drought frequencies revealed by a four-century-long tree-ring isotopic record from Brittany, western France, Climate Dynamics, 24, 57-69, 2005.

Masson-Delmotte, V., Steen-Larsen, H. C., Ortega, P., Swingedouw, D., Popp, T., Vinther, B. M., Oerter, H., Sveinbjornsdottir, A. E., Gudlaugsdottir, H., Box, J. E., Falourd, S., Fettweis, X., Gallée, H., Garnier, E., Gkinis, V., Jouzel, J., Landais, A., Minster, B., Paradis, N., Orsi, A., Risi, C., Werner, M., and White, J. W. C.: Recent changes in north-west Greenland climate documented by NEEM shallow ice core data and simulations, and implications for past-temperature reconstructions, The Cryosphere, 9, 1481-1504, 10.5194/tc-9-1481-2015, 2015.

McCarroll, D., and Loader, N. J.: Stable isotopes in tree rings, Quaternary Science Reviews, 23, 771-801, 10.1016/j.quascirev.2003.06.017, 2004.

McDermott, F.: Palaeo-climate reconstruction from stable isotope variations in speleothems: a review, Quaternary Science Reviews, 23, 901-918, 10.1016/j.quascirev.2003.06.021, 2004.

Miller, D. L., Mora, C. I., Grissino-Mayer, H. D., Mock, C. J., Uhle, M. E., and Sharp, Z.: Tree-ring isotope records of tropical cyclone activity, Proceedings of the National Academy of Sciences, 103, 14294-14297, 10.1073/pnas.0606549103, 2006.

Monteith, J. L.: A Reinterpretation of Stomatal Responses to Humidity, Plant, Cell and Environment, 18, 357-364, 1995.

Murray, S. J., Foster, P. N., and Prentice, I. C.: Evaluation of global continental hydrology as simulated by the Land-surface Processes and eXchanges Dynamic Global Vegetation Model, Hydrology and Earth System Sciences, 15, 91-105, 2011.

Noone, D., and Simmonds, I.: Associations between $\delta^{18}O$ of water and climate parameters in a simulation of atmospheric circulation for 1979-95, Journal of Climate, 15, 3150-3169, 2002.

Offermann, C., Pedro Ferrio, J., Holst, J., Grote, R., Siegwolf, R., Kayler, Z., and Gessler, A.: The long way down-are carbon and oxygen isotope signals in the tree ring uncoupled from canopy physiological processes?, Tree Physiology, 31, 1088-1102, 2011.

Ogée, J., Barbour, M. M., Wingate, L., Bert, D., Bosc, A., Stievenard, M., Lambrot, C., Pierre, M., Bariac, T., Loustau, D., and Dewar, R. C.: A single-substrate model to interpret intra-annual stable isotope signals in tree-ring cellulose, Plant Cell and Environment, 32, 1071-1090, 2009.

Prentice, I. C., Kelley, D. I., Foster, P. N., Friedlingstein, P., Harrison, S. P., and Bartlein, P. J.: Modeling fire and the terrestrial carbon balance, Global Biogeochemical Cycles, 25, GB3005, 2011.

Raddatz, T. J., Reick, C. H., Knorr, W., Kattge, J., Roeckner, E., Schnur, R., Schnitzler, K. G., Wetzel, P., and Jungclaus, J.: Will the tropical land biosphere dominate the climate-carbon cycle feedback during the twenty-first century?, Climate Dynamics, 29, 565-574, 2007.

Reynolds-Henne, C. E., Siegwolf, R. T. W., Treydte, K. S., Esper, J., Henne, S., and Saurer, M.: Temporal stability of climate-isotope relationships in tree rings of oak and pine (Ticino, Switzerland), Global Biogeochemical Cycles, 21, 2007.

Rinne, K. T., Loader, N. J., Switsur, V. R., and Waterhouse, J. S.: 400-year May-August precipitation reconstruction for Southern England using oxygen isotopes in tree rings, Quaternary Science Reviews, 60, 13-25, 2013.

Ripullone, F., Matsuo, N., Stuart-Williams, H., Wong, S. C., Borghetti, M., Tani, M., and Farquhar, G.: Environmental Effects on Oxygen Isotope Enrichment of Leaf Water in Cotton Leaves, Plant Physiology, 146, 729-736, 2008.

Risi, C., Bony, S., Vimeux, F., and Jouzel, J.: Water-stable isotopes in the LMDZ4 general circulation model: Model evaluation for present-day and past climates and applications to climatic interpretations of tropical isotopic records, Journal of Geophysical Research-Atmospheres, 115, D12118, 2010.

Roden, J. S., Lin, G. G., and Ehleringer, J. R.: A mechanistic model for interpretation of hydrogen and oxygen isotope ratios in tree-ring cellulose, Geochimica Et Cosmochimica Acta, 64, 21-35, 10.1016/S0016-7037(99)00195-7, 2000.

Roeckner, E., Bäuml, G., Bonaventura, L., Brokopf, R., Esch, M., Giorgetta, M., Hagemann, S., Kirchner, I., Kornblueh, L., Manzini, E., Rhodin, A., Schlese, U., Schulzweida, U., and Tompkins, A.: The atmospheric general circulation model ECHAM5 - Part 1, Max-Planck-Institut für Meteorologie, Report No. 349, 2003.

Rozanski, K., Araguasaraguas, L., and Gonfiantini, R.: Relation between long-term trends of $^{18}O$ isotope composition of precipitation and climate, Science, 258, 981-985, 1992.

Ruosch, M., Spahni, R., Joos, F., Henne, P. D., van der Knaap, P., and Tinner, W.: Past and future evolution of *Abies alba* forests in Europe – comparison of a dynamic vegetation model with palaeo data and observations, Global Change Biology, 22, 727-740, 2016.

Sarris, D., Siegwolf, R., and Körner, C.: Inter- and intra-annual stable carbon and oxygen isotope signals in response to drought in Mediterranean pines, Agricultural and Forest Meteorology, 168, 59-68, 2013.

Saurer, M., Schweingruber, F., Vaganov, E. A., Shiyatov, S. G., and Siegwolf, R.: Spatial and temporal oxygen isotope trends at the northern tree-line in Eurasia, Geophysical Research Letters, 29, 7-1, 10.1029/2001GL013739, 2002.

Saurer, M., Spahni, R., Frank, D. C., Joos, F., Leuenberger, M., Loader, N. J., McCarroll, D., Gagen, M., Poulter, B., Siegwolf, R. T. W., Andreu-Hayles, L., Boettger, T., Dorado Linan, I., Fairchild, I. J., Friedrich, M., Gutierrez, E., Haupt, M., Hilasvuori, E., Heinrich, I., Helle, G., Grudd, H., Jalkanen, R., Levanic, T., Linderholm, H. W., Robertson, I., Sonninen, E., Treydte, K., Waterhouse, J. S., Woodley, E. J., Wynn, P. M., and Young, G. H. F.: Spatial variability and temporal trends in water-use efficiency of European forests, Global Change Biology, 20, 3700-3712, 2014.

Schär, C., Vidale, P. L., Lüthi, D., Frei, C., Häberli, C., Liniger, M. A., and Appenzeller, C.: The role of increasing temperature variability in European summer heatwaves, Nature, 427, 332-336, 2004.

Severinghaus, J. P., Beaudette, R., Headly, M. A., Taylor, K., and Brook, E. J.: Oxygen-18 of $O_2$ Records the Impact of Abrupt Climate Change on the Terrestrial Biosphere, Science, 324, 1431-1434, 2009.

Shackleton, N. J., and Obdyke, N. D.: Oxygen-isotope and paleomagnetic stratigraphy of equatorial Pacific core V28–238: oxygen-isotope temperatures and ice volumes on an $10^5$ year to $10^6$ year scale, Quaternary Research, 3, 39-55, 1973.

Sidorova, O. V., Siegwolf, R. T. W., Saurer, M., Naurzbaev, M. M., and Vaganov, E. A.: Isotopic composition ($\delta^{13}C$, $\delta^{18}O$) in wood and cellulose of Siberian larch trees for early Medieval and recent periods, Journal of Geophysical Research-Biogeosciences, 113, G02019, 2008.

Sitch, S., Smith, B., Prentice, I. C., Arneth, A., Bondeau, A., Cramer, W., Kaplan, J. O., Levis, S., Lucht, W., Sykes, M. T., Thonicke, K., and Venevsky, S.: Evaluation of ecosystem dynamics, plant geography and terrestrial carbon cycling in the LPJ dynamic global vegetation model, Global Change Biology, 9, 161-185, 10.1046/j.1365-2486.2003.00569.x, 2003.

Sjolte, J., Hoffmann, G., Johnsen, S. J., Vinther, B. M., Masson-Delmotte, V., and Sturm, C.: Modeling the water isotopes in Greenland precipitation 1959–2001 with the meso-scale model REMO-iso, Journal of Geophysical Research: Atmospheres, 116, 1-22, 10.1029/2010jd015287, 2011.

Song, X., Clark, K. S., and Helliker, B. R.: Interpreting species-specific variation in tree-ring oxygen isotope ratios among three temperate forest trees, Plant, Cell & Environment, 37, 2169-2182, 2014.

Spahni, R., Joos, F., Stocker, B. D., Steinacher, M., and Yu, Z. C.: Transient simulations of the carbon and nitrogen dynamics in northern peatlands: from the Last Glacial Maximum to the 21st century, Clim. Past, 9, 1287-1308, 10.5194/cp-9-1287-2013, 2013.

Sternberg, L., and Ellsworth, P. F. V.: Divergent Biochemical Fractionation, Not Convergent Temperature, Explains Cellulose Oxygen Isotope Enrichment across Latitudes, PLoS ONE, 6, e28040, 2011.

Sternberg, L. d. S. L., DeNiro, M. J., and Savidge, R. A.: Oxygen Isotope Exchange between Metabolites and Water during Biochemical Reactions Leading to Cellulose Synthesis, Plant Physiology, 82, 423-427, 1986.

Sternberg, L. d. S. L.: Comment on "Oxygen isotope ratios ($^{18}O/^{16}O$) of hemicellulose-derived sugar biomarkers in plants, soils and sediments as paleoclimate proxy I: Insight from a climate chamber experiment" by Zech et al. (2014), Geochimica Et Cosmochimica Acta, 141, 677-679, 2014.

Sternberg, L. d. S. L. O. R.: Oxygen stable isotope ratios of tree-ring cellulose: the next phase of understanding, New Phytologist, 181, 553-562, 10.1111/j.1469-8137.2008.02661.x, 2009.

Stocker, B. D., Roth, R., Joos, F., Spahni, R., Steinacher, M., Zaehle, S., Bouwman, L., Xu, R., and Prentice, I. C.: Multiple greenhouse-gas feedbacks from the land biosphere under future climate change scenarios, Nature Climate Change, 3, 666-672, 2013.

Sturm, K., Hoffmann, G., Langmann, B., and Stichler, W.: Simulation of $\delta^{18}O$ in precipitation by the regional circulation model $REMO_{iso}$, Hydrological Processes, 19, 3425–3444, 10.1002/hyp.5979, 2005.

Treydte, K., Frank, D., Esper, J., Andreu, L., Bednarz, Z., Berninger, F., Boettger, T., D'Alessandro, C. M., Etien, N., Filot, M., Grabner, M., Guillemin, M. T., Gutierrez, E., Haupt, M., Helle, G., Hilasvuori, E., Jungner, H., Kalela-Brundin, M., Krapiec, M., Leuenberger, M., Loader, N. J., Masson-Delmotte, V., Pazdur, A., Pawelczyk, S., Pierre, M., Planells, O., Pukiene, R., Reynolds-Henne, C. E., Rinne, K. T., Saracino, A., Saurer, M., Sonninen, E., Stievenard, M., Switsur, V. R., Szczepanek, M., Szychowska-Krapiec, E., Todaro, L., Waterhouse, J. S., Weigl, M., and Schleser, G. H.: Signal strength and climate calibration of a European tree-ring isotope network, Geophysical Research Letters, 34, 2007.

Treydte, K., Boda, S., Pannatier, E. G., Fonti, P., Frank, D., Ullrich, B., Saurer, M., Siegwolf, R., Battipaglia, G., Werner, W., and Gessler, A.: Seasonal transfer of oxygen isotopes from precipitation and soil to the tree ring: source water versus needle water enrichment, New Phytologist, 202, 772-783, 2014.

Treydte, K. S., Schleser, G. H., Helle, G., Frank, D. C., Winiger, M., Haug, G. H., and Esper, J.: The twentieth century was the wettest period in northern Pakistan over the past millennium, Nature, 440, 1179-1182, 10.1038/nature04743, 2006.

Wang, X. F., Yakir, D., and Avishai, M.: Non-climatic variations in the oxygen isotopic compositions of plants, Global Change Biology, 4, 835-849, 1998.

Wania, R., Ross, I., and Prentice, I. C.: Integrating peatlands and permafrost into a dynamic global vegetation model: 2. Evaluation and sensitivity of vegetation and carbon cycle processes, Global Biogeochemical Cycles, 23, GB3015, 2009.

Waterhouse, J. S., Switsur, V. R., Barker, A. C., Carter, A. H. C., and Robertson, I.: Oxygen and hydrogen isotope ratios in tree rings: how well do models predict observed values?, Earth and Planetary Science Letters, 201, 421-430, 10.1016/S0012-821X(02)00724-0, 2002.

Weigt, R. B., Bräunlich, S., Zimmermann, L., Saurer, M., Grams, T. E. E., Dietrich, H.-P., Siegwolf, R. T. W., Nikolova, P. S.: Comparison of $\delta^{18}O$ and $\delta^{13}C$ values between tree-ring whole wood and cellulose in five species growing under two different site conditions, Rapid Communications in Mass Spectrometry, 29, 2233–2244, 2015.

Werner, M., Langebroek, P. M., Carlsen, T., Herold, M., and Lohmann, G.: Stable water isotopes in the ECHAM5 general circulation model: Toward high-resolution isotope modeling on a global scale, Journal of Geophysical Research-Atmospheres, 116, D15109, 2011.

Wershaw, R. L., Friedman, I., Heller, S. J., and Frank, P. A.: Hydrogen isotope fractionation of water passing through trees, in: Advances in organic geochemistry, edited by: Hobson, G. D., Pergamon Press, Oxford, 55-67, 1966.

West, J. B., Sobek, A., and Ehleringer, J. R.: A Simplified GIS Approach to Modeling Global Leaf Water Isoscapes, PLoS ONE, 3, e2447, 2008.

988 Xu, G., Liu, X., Qin, D., Chen, T., Wang, W., Wu, G., Sun, W., An, W., and Zeng, X.: Relative
989 humidity reconstruction for northwestern China's Altay Mountains using tree-ring $\delta^{18}O$, Chinese
990 Science Bulletin, 59, 190-200, 2014.

991 Zech, M., Mayr, C., Tuthorn, M., Leiber-Sauheitl, K., and Glaser, B.: Reply to the comment of
992 Sternberg on "Zech et al. (2014) Oxygen isotope ratios ($^{18}O/^{16}O$) of hemicellulose-derived sugar
993 biomarkers in plants, soils and sediments as paleoclimate proxy I: Insight from a climate chamber
994 experiment. GCA 126, 614-623.", Geochimica Et Cosmochimica Acta, 141, 680-682, 2014.

995
996

997 Table 1. Comparison of input data and simulations by LPX-Bern (Model) against measurements
998 (Observed) performed at two sites (LOV, LOT) in the Lötschen Valley (Switzerland) for
999 averages across June, July, and August 2008. Because the two sites lie within the same grid cell
1000 of LPX-Bern, the simulated data are identical.

1001

| Parameter | Observed | | Model |
|---|---|---|---|
| | LOV | LOT | LPX-Bern |
| Air temperature [°C] | 15.4 | 11.1 | 16.5 |
| Relative humidity [%] | 75.6 | 72.6 | 78.5 |
| Precipitation [mm] | 251.5 | 294.8 | 387.0 |
| Soil water $\delta^{18}O$ [‰] | -6.1 | -8.6 | -7.8 |
| Needle water $\delta^{18}O$ [‰] | 10.6 | 3.0 | 6.5 |
| Stem cellulose $\delta^{18}O$ [‰] | 29.2 | 29.0 | 27.3 |
| Enrichment of needle water above source [‰] | 16.7 | 11.6 | 14.3 |
| Enrichment of stem cellulose above needle water [‰] | 18.6 | 26.0 | 20.8 |
| Enrichment of stem cellulose above source [‰] | 35.3 | 37.6 | 35.1 |

1002

1003

1004 Table 2. Effect of a 10% increase in parameter values/input data on simulated stem cellulose $\delta^{18}O$
1005 at site DAV for the June, July, and August 1960 average.

1006

| Parameter | Change in stem cellulose $\delta^{18}O$ [‰] |
|---|---|
| Air temperature [ºC] | -0.2 |
| Relative humidity | -6.7 |
| $\varepsilon_k$ | 1.7 |
| $\varepsilon^+$ | 2.3 |
| Transpiration (E) | -0.3 |
| Path length (L) | -0.3 |
| Péclet number ($\wp$) | -0.3 |
| $p_{ex}$ | -1.9 |
| $\delta^{18}O_{sw}$ | 2.4 |
| $\delta^{18}O_{wv}$ | 2.9 |

1007

1008

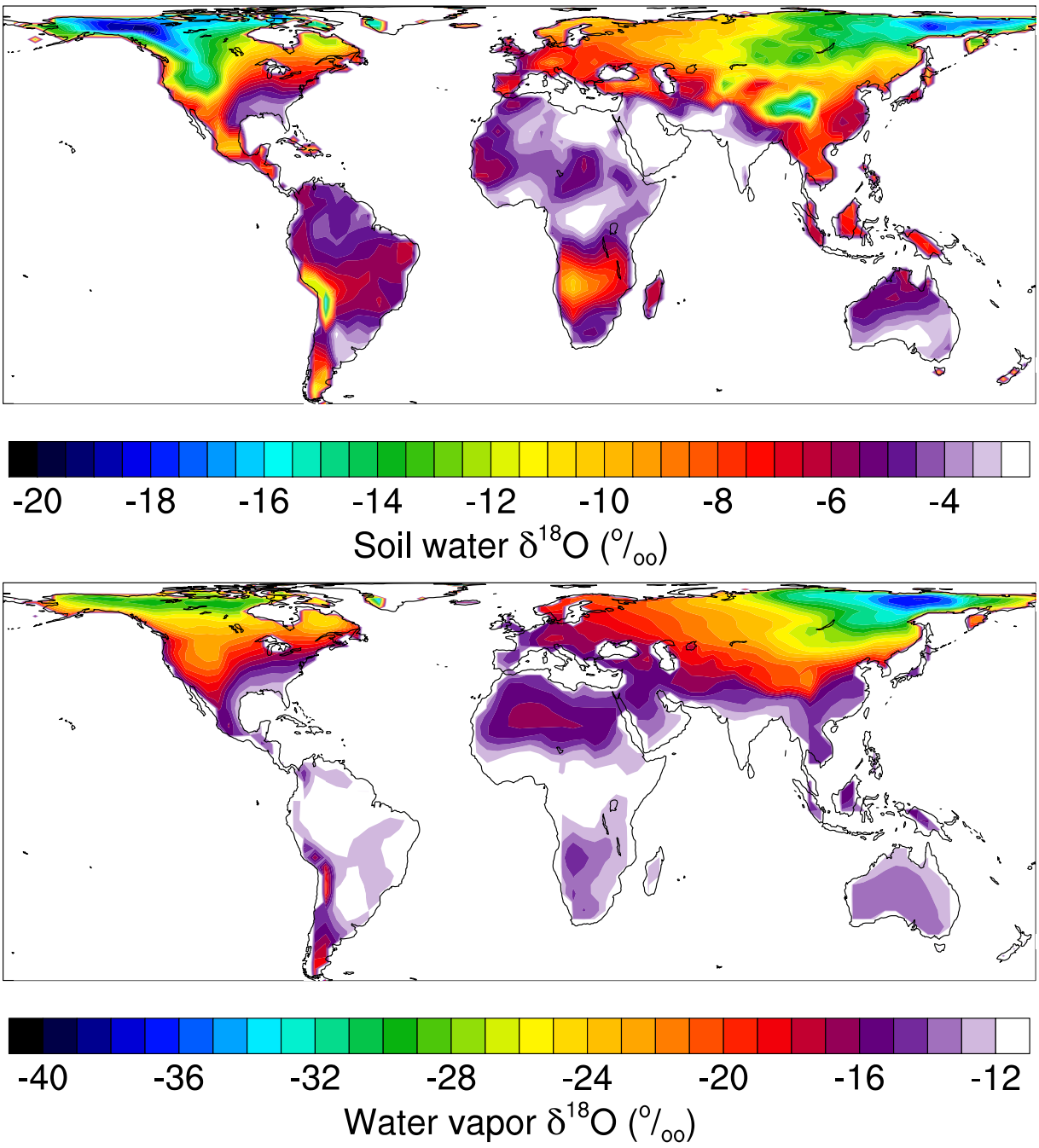


Figure 1. Simulated monthly soil water $\delta^{18}O$ (upper panel) and water vapor $\delta^{18}O$ (lower panel) was used as input data for the calculation of leaf water and cellulose $\delta^{18}O$ by LPX-Bern. The presented data were simulated by the coupled atmosphere-land surface model ECHAM5-JSBACH (Haese et al. 2013). Average values for 1961-1990 are shown.

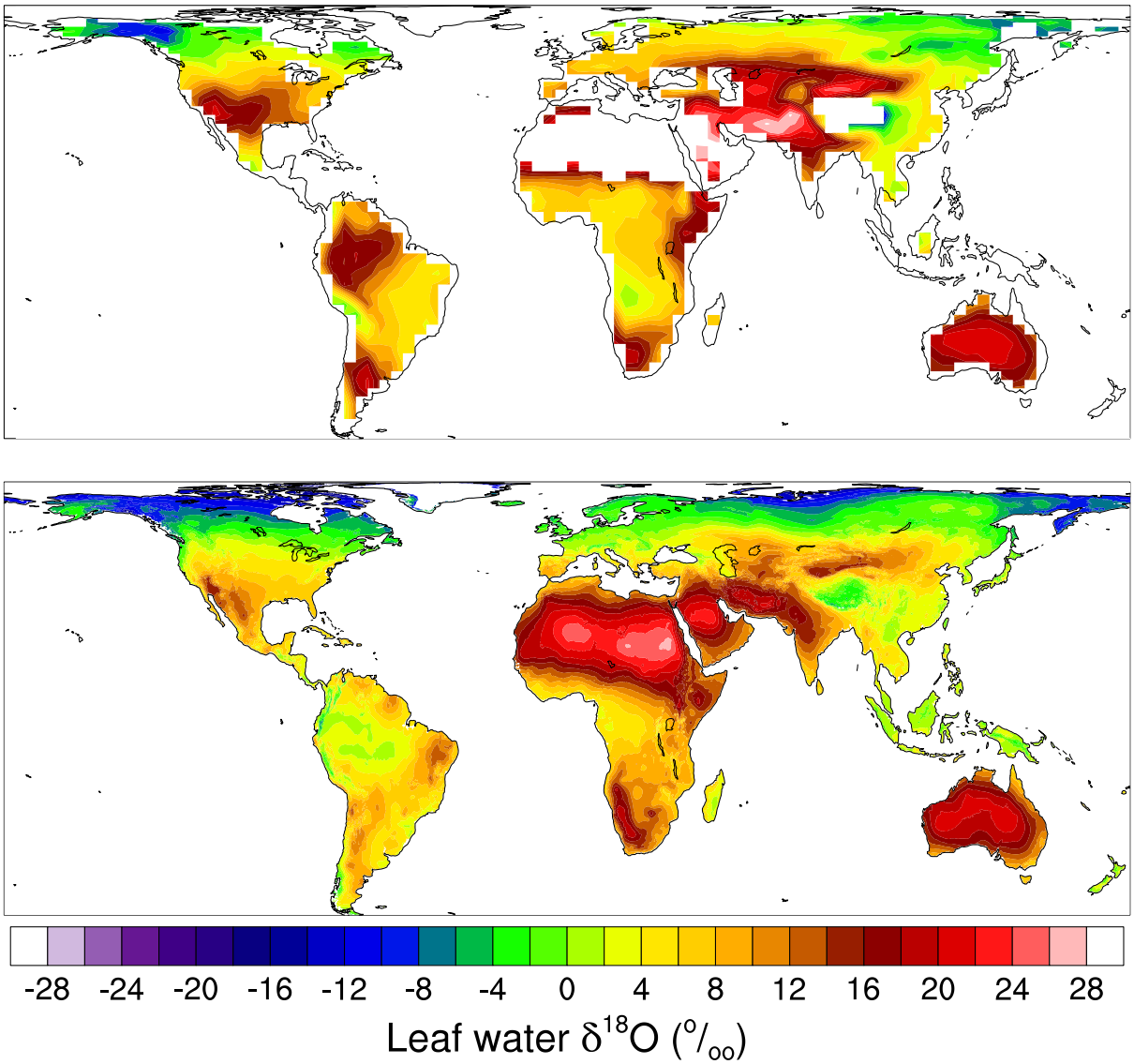


Figure 2. Leaf water $\delta^{18}O$ (‰) as simulated by LPX-Bern (upper panel) compared to results by West et al. (2008) using a GIS approach (lower panel). LPX-Bern results are shown for the years 1961-1990 using the Craig-Gordon formulation (i.e. no Péclet effect) for comparability and for all plant functional types including grasses and herbs.

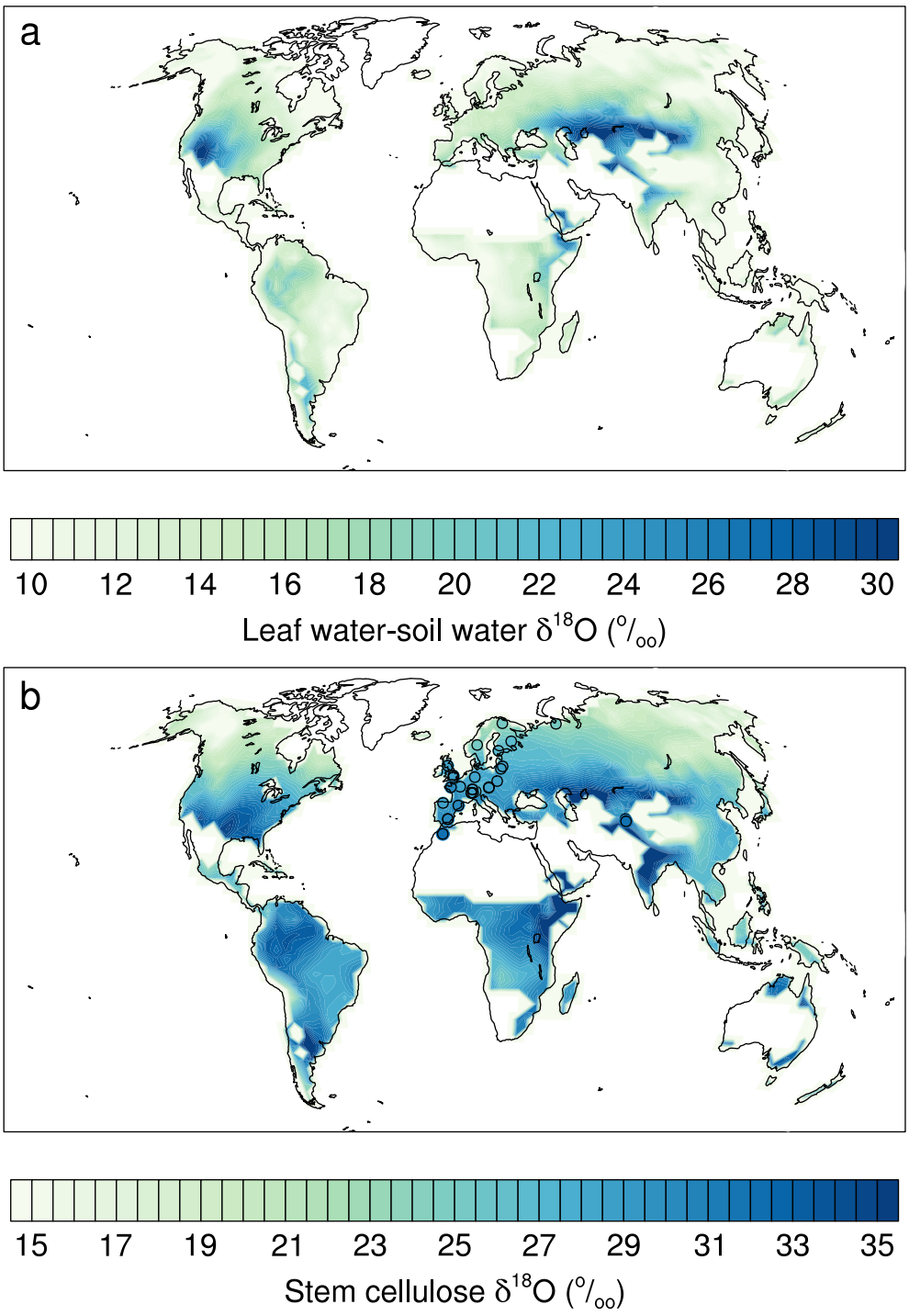


1023

1024 Figure 3. Leaf water $^{18}O$ enrichment above soil water $\delta^{18}O$ (a) and stem cellulose $\delta^{18}O$ (b)
1025 averaged over all tree plant functional types and over 1961-2012 as simulated by LPX-Bern.
1026 Colored circles in panel b show temporally-averaged results from local tree ring data (Table S1 in
1027 the Supplement) on the same color scale as model results.

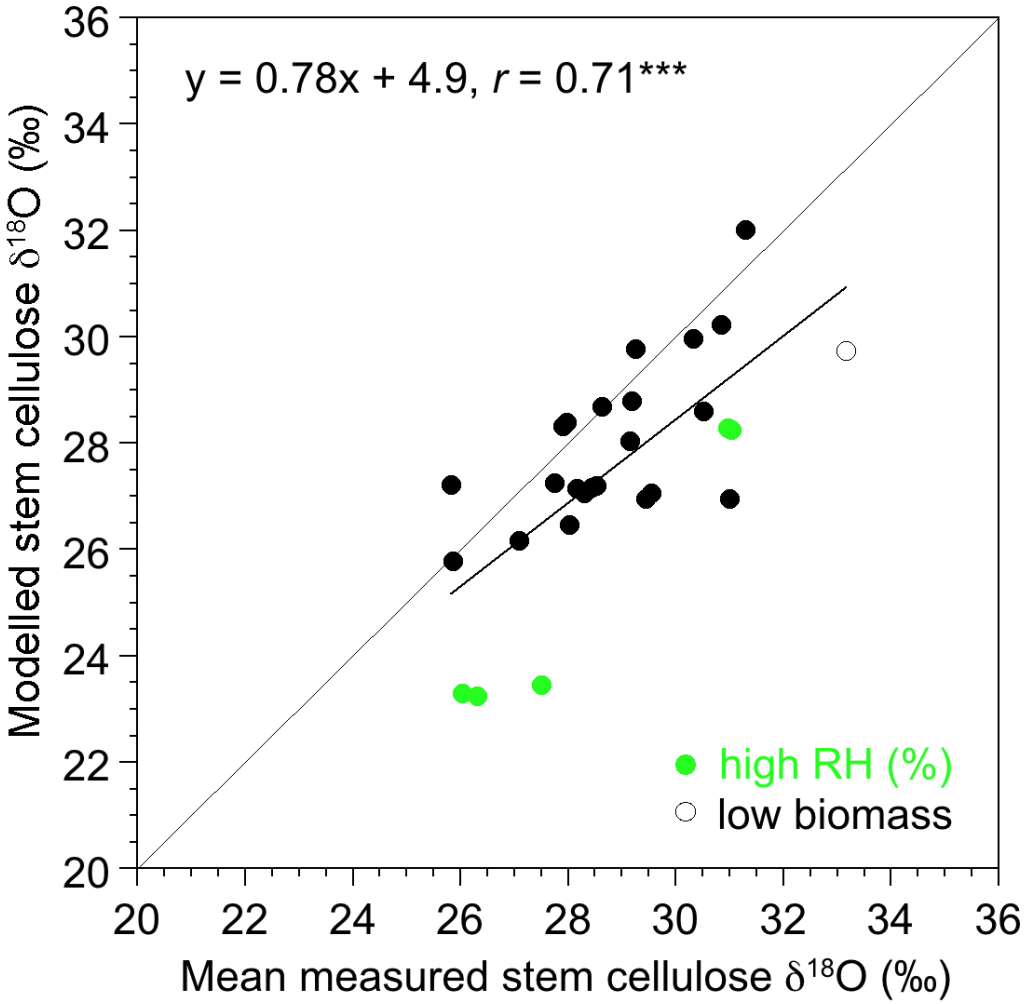


Figure 4. Comparison of simulated and measured stem cellulose $\delta^{18}O$ for 31 sites in temperate and boreal forests (mainly in Europe). Each symbol represents the mean over the years 1960-2003 (or up to 2012 if available) for a specific species (e.g. *Quercus petraea* (Matt.) Liebl., Table S1) and the corresponding plant functional type in LPX-Bern. Sites where the relative humidity forcing has very high values (>80%) are highlighted in light green. The open symbol reflects a single site (CAZ) where simulated above ground biomass is very low. See supplementary online material for location and description of sites (Table S1). Pearson's correlation coefficient (*r*) and the significance level (***, $P < 0.001$) were calculated including all sites.

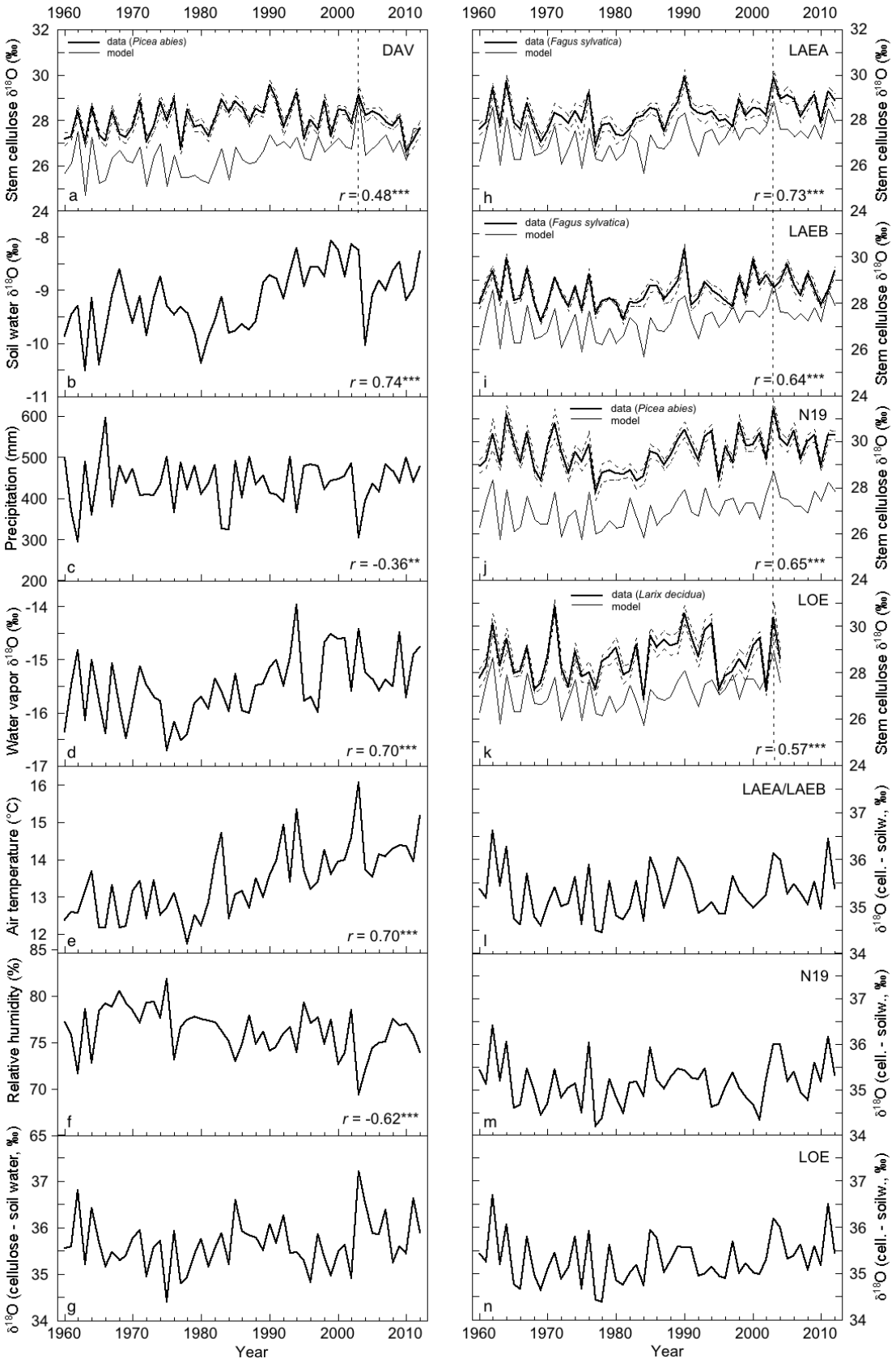
1960
1970
1980
1990
2000
2010
data (Picea abies)
model
DAV
Stem cellulose δ18O (‰)
a
r = 0.48***
Soil water δ18O (‰)
b
r = 0.74***
Precipitation (mm)
c
r = -0.36**
Water vapor δ18O (‰)
d
r = 0.70***
Air temperature (°C)
e
r = 0.70***
Relative humidity (%)
f
r = -0.62***
δ18O (cellulose - soil water, ‰)
g
Year
data (Fagus sylvatica)
model
LAEA
h
r = 0.73***
LAEB
i
r = 0.64***
data (Picea abies)
model
N19
j
r = 0.65***
data (Larix decidua)
model
LOE
k
r = 0.57***
LAEA/LAEB
l
δ18O (cell. - soilw., ‰)
N19
m
LOE
n
Year

1039

1040 Figure 5. Comparison of measured (data) and simulated (model) stem cellulose $\delta^{18}O$ (panels a, h-
1041 k) for the alpine sites Davos (DAV), and Lötschen Valley (N19, LOE), and sites Lägern (LAEA,
1042 LAEB) in the Swiss Central Plateau. Standard errors (dashed lines) are based on measurements
1043 of ten trees. Panels b-f show input data as used for the simulation of stem cellulose $\delta^{18}O$ in LPX-
1044 Bern for site DAV (average of June, July, and August is presented). The vertical dashed line
1045 highlights the extremely hot summer 2003. Pearson's correlation coefficients, *r*, with simulated
1046 stem cellulose $\delta^{18}O$ are shown. Significance levels for the correlations are (*, $P < 0.05$; **, $P <$
1047 0.01., ***, $P < 0.001$). Panels g and l-n show the $^{18}O$-enrichment in stem cellulose above soil
1048 water $\delta^{18}O$. Note that in LPX-Bern sites LAEA, LAEB, N19, and LOE lie within the same grid
1049 cell but are represented by different tree functional types (broad-leaved deciduous (LAEA,
1050 LAEB), needle-leaved evergreen (N19), and needle-leaved deciduous (LOE)).
1051

1052

1053

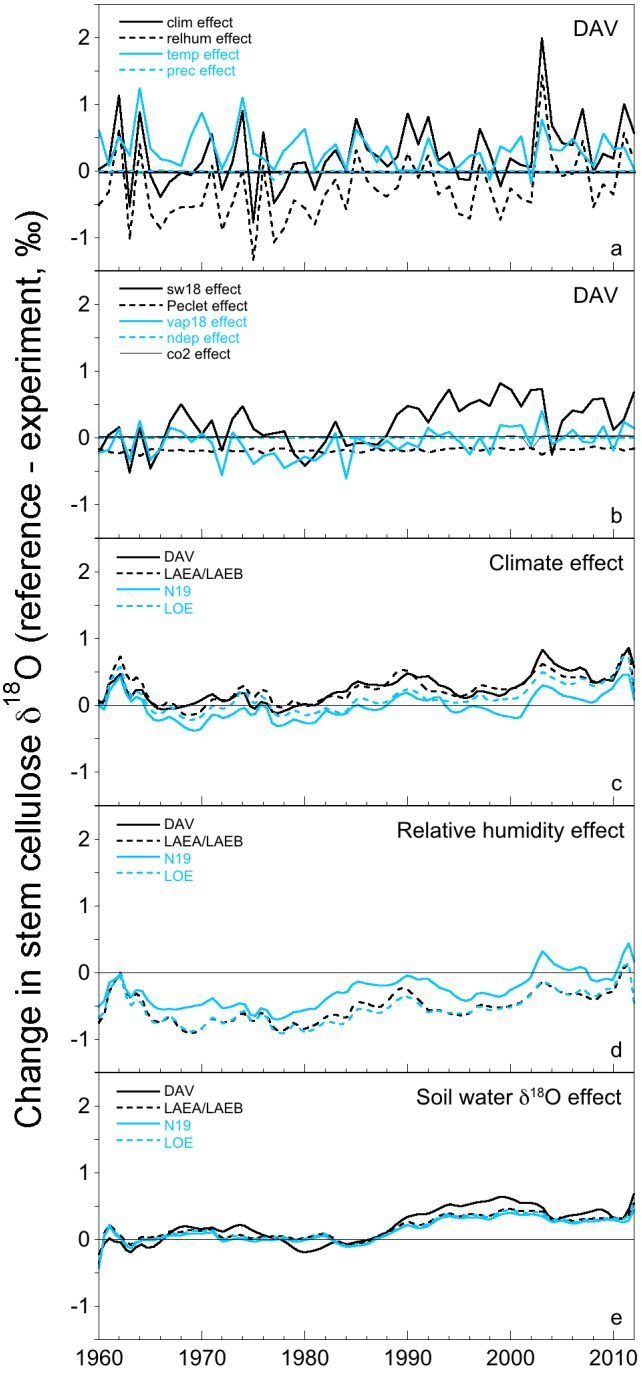


1054

Figure 6. Influence of forcing factors and the Péclet parameterization on simulated $\delta^{18}O$ of stem cellulose. Panels a and b show results for the alpine site in Davos (DAV) and for all factors investigated. Panels c, d, and e each show the influence of one individual, major driver for five sites, located within the Swiss Central Plateau (Lägeren (LAEA and LAEB, black, dashed line)), and the high-elevation sites in the Lötschen Valley (N19, blue, solid; LOE; blue, dashed) and in Davos (DAV, black solid). Each curve shows the differences in $\delta^{18}O$ of stem cellulose between the reference simulation (all forcings vary) and one sensitivity simulation (one forcing factor is kept constant). Constant forcing factors include relative humidity (relhum effect), air temperature (temp effect), precipitation (prec effect), soil water $\delta^{18}O$ (sw18 effect), water vapor $\delta^{18}O$ (vap18 effect), atmospheric nitrogen deposition (ndep effect), atmospheric $CO_2$ (co2 effect)) or a combination of constant forcings (climate (clim effect), i.e., temperature, precipitation, cloud cover, and number of wet days). An additional simulation is run without the Péclet effect (Peclet effect). The curves are smoothed with Stineman functions in panels c, d, and, e.

1069

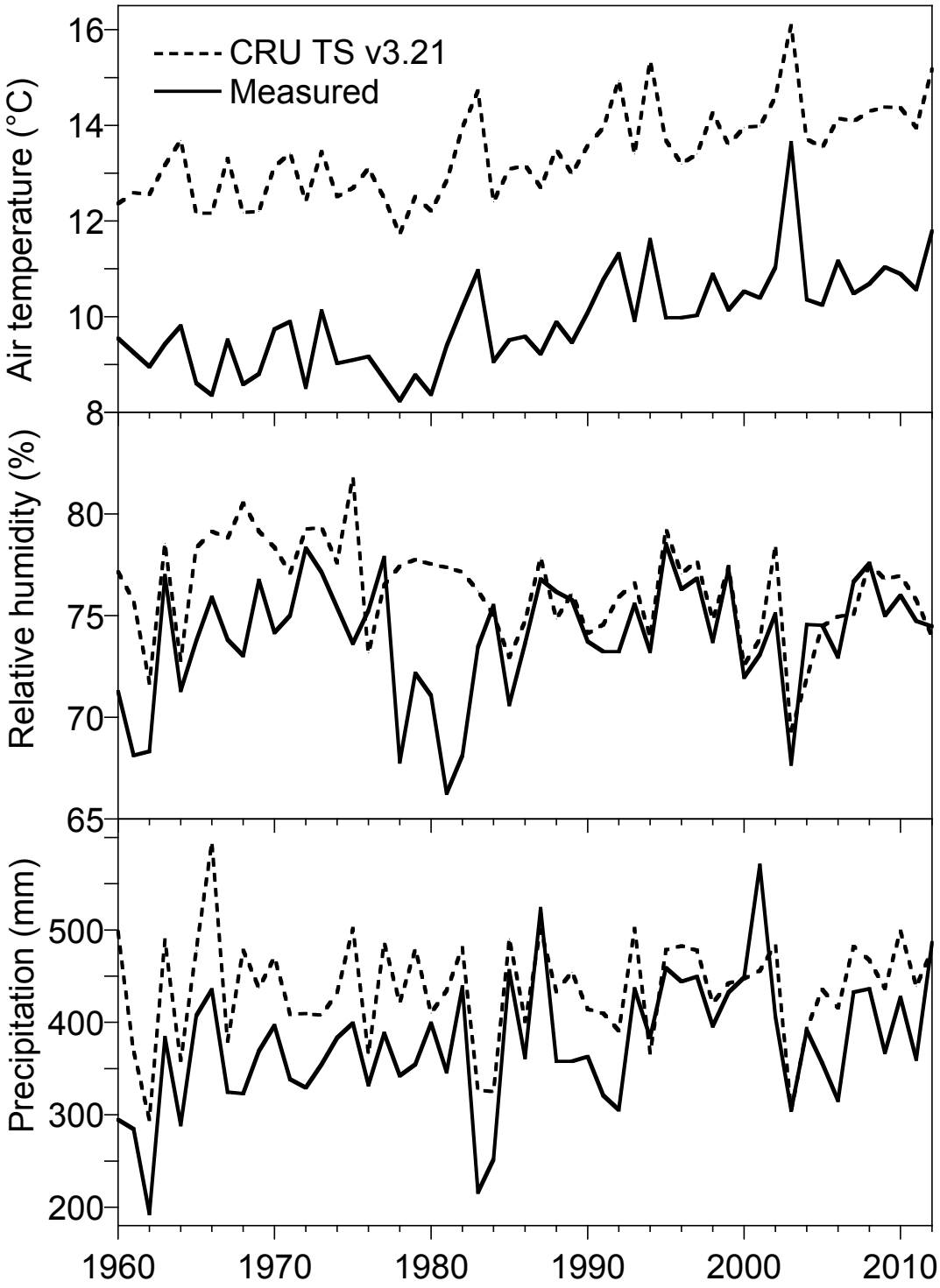
CRU TS v3.21
Measured
Air temperature (°C)
16
14
12
10
8
Relative humidity (%)
80
75
70
65
Precipitation (mm)
500
400
300
200
1960
1970
1980
1990
2000
2010

1070

Figure 7. Comparison of climate input data for the alpine site Davos (DAV). Solid lines show grid cell average data from the CRU climatology (CRU TS v3.21) as used in our standard model setup. Dashed lines show data from a nearby meteorological station as used in a sensitivity simulation (run 'ewcTmeteo' in Fig. 8). Temperature is warmer and precipitation higher in the grid cell average data compared to the local data.

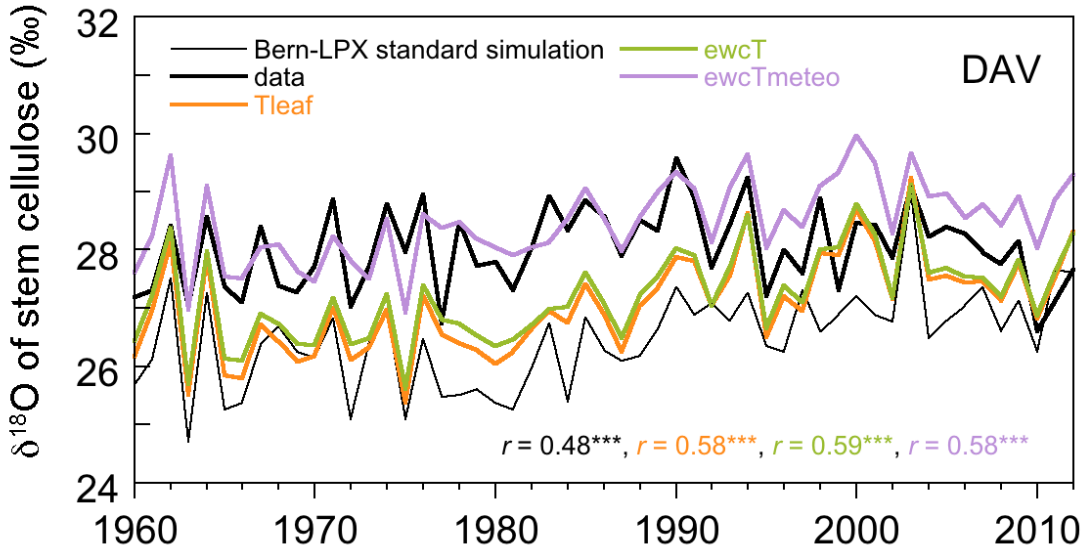


Figure 8. Effect of reduced leaf temperature and a temperature dependent biochemical fraction ($\varepsilon_{wc}$) on simulated stem cellulose $\delta^{18}O$ for site DAV (Davos). Leaf temperature was decreased by 3.5°C relative to air temperature ('Tleaf') because at site DAV, measured air temperature was on average 3.5°C lower than temperature from CRU TS v.3.21 used in the model ('LPX-Bern standard simulation'). The temperature dependent biochemical fraction was tested with the air temperature from CRU ('ewcT') and with measured air temperature from a nearby meteorological station ('ewcTmeteo'). Pearson's correlation coefficients, r, with measured stem cellulose $\delta^{18}O$ are shown. Significance levels for the correlations are (*, $P < 0.05$; **, $P < 0.01$; ***, $P < 0.001$).